Reduced Kinetic Schemes of Complex Reaction Systems: Fossil and Biomass-Derived Transportation Fuels

ELISEO RANZI, ALESSIO FRASSOLDATI, ALESSANDRO STAGNI, MATTEO PELUCCHI, ALBERTO CUOCI, TIZIANO FARAVELLI

Dipartimento CMIC, *Politecnico di Milano*, *Politecnico di Milano*, *Milan*, *Italy*

Received 11 March 2014; revised 19 May 2014; accepted 20 May 2014

Correspondence to: Eliseo Ranzi; e-mail: eliseo.ranzi@polimi.it.
Contract grant sponsor: MSE and CNR-DIITET.
Contract grant number: Project D44G12000040001. Supporting Information is available in the online.

INTRODUCTION

Liquid transportation fuels remain one of the most important energy sources. Currently, 85% of U.S. energy comes from hydrocarbon sources, including natural gas, petroleum, and coal; 97% of transportation energy derives from petroleum, essentially all from combustion in gasoline engines (65%), diesel engines (20%), and jet turbines (12%) [1]. Independently on external or geopolitical factors, the internal combustion engine will remain the primary driver of transport for the next 30–50 years. The nature of transportation technologies offers the opportunity for improvements in efficiency of 25–50% through technical investment in advanced fuel and engine technology. As clearly summarized by Bunting [2], the automotive and engine industries are in a period of very rapid change being driven by new combustion strategies, the introduction of new fuels, new emission standards, and push for increased efficiency. These changes lead to the need for optimal design and modeling of engine combustion and performance. New combustion strategies include homogeneous charge compression ignition (HCCI), partial-premixed combustion compression ignition (PCCI), and dilute low-temperature combustion, which are being developed for lower emissions and improved fuel economy. New fuels include biofuels, such as ethanol or biodiesel, and those derived from new crude oil sources, such as gas to liquids, coal to liquids, oil sands, oil shale, and wet natural gas. A better understanding of combustion kinetics and the proper use of reliable mathematical models can aid decisions not simply on engine design but also on fuel properties to maximize engine performance and minimize emissions. For example, once optimal fuel characteristics are defined, researchers can use the predictive model to evaluate the impact of including new groups of compounds in a fuel formulation [3]. The Cluster of Excellence "Tailor-Made Fuels from Biomass" (TMFB) at RWTH Aachen University was established in 2007 to develop new, biomass-based, synthetic fuels for mobile applications and to determine the best possible combination of fuel components, whose properties are derived from the requirements of future combustion processes [4].

Recently, new European regulations pushed toward a greater use of renewable fuels to reduce greenhouse gases (GHG) emissions for transport, improve energy security and efficiency. Ten percent of transportation fuels on an energy basis is a fixed and mandatory target, and it must be derived from sustainably produced, renewable sources by 2020. This percentage can include the use of bioblending components, renewable electricity for vehicle recharging, biogas from waste materials, and other policies. Over the same time horizon, the fuel suppliers must reduce the GHG emissions of transportation fuels by at least 6% in 2020, compared to a 2010 baseline, primarily by blending certified bioderived components [5]. Thus, the coming decade, and not only for European road transport, will be characterized by the implementation of legislative targets that will impact car manufacturers, vehicle technology, refineries, and biofuel producers. Internal combustion engine will have to respect tighter regulations on emissions of CO_2 and air pollutants (polycyclic aromatic hydrocarbons [PAH], soot, NOx, SOx, etc.). Conventional biofuels are widely available, but they are accompanied by sustainability concerns in the face of increasing demand. Compatibility with higher biofuel blends is still to be proven, requiring time, testing efforts, and investments [6].

The kinetic modeling of the combustion process for these new fuels and combustion regimes is necessary to allow modeling and performance assessment for engine design purposes. Liquid fossil and biofuels contain varying blends of many hydrocarbons. There has been a recent collaborative effort to develop surrogate models to emulate real fuels to accurately predict combustion properties [1]. Such surrogate models typically contain mixtures of a small number of reference liquid hydrocarbons. However, detailed reaction mechanisms for surrogates of gasoline, jet, and diesel fuels typically contain large numbers of species and reactions. Despite rapid advancements in computing power, it is a difficult task to integrate such detailed reaction mechanisms into large-scale computational simulations in terms of CPU time and memory requirements. Since the computational cost of chemistry scales by the third power of the number of species, the large sizes of detailed kinetic schemes could pose

problems even in one-dimensional (1D) modeling. In addition, the wide range of time scales and the nonlinear coupling between species and reactions induces stiffness when solving balance equations [7].

COMPLEXITY OF THE TRANSPORTATION FUELS AND SURROGATE MIXTURES

Liquid transportation fuels are constituted by complex hydrocarbon mixtures derived from refinery. These mixtures contain hundreds of large hydrocarbon species that meet general physical properties and chemical specifications. The behavior of multicomponent transportation fuels is more complicated than single component fuels not only because the species produced from one component can react with other components, but mainly because the original fuels are difficult to be characterized and scarcely reproducible. Owing to this complexity, surrogate mixtures were introduced to better study and analyze the combustion behavior of gasoline, of kerosene, and diesel fuels. Surrogate mixtures are well-defined mixtures of a limited number of reference components, usefully applied to mimic the behavior of real fuels in respect of particular investigation target. Fuel surrogates may be defined as physical or chemical surrogates depending on whether the surrogate mixture has the similar physical or chemical properties as the fuel to be studied. Chemical properties include the right proportion of aromatics, naphthenes, and paraffins [8]. Physical properties include volatility, heat of combustion, freeze point, and so on. Surrogate mixtures involve a small number of chemical compounds containing most of the functional groups in realistic fuels [9]. Physical and combustion properties of the different fuels can be met by a large variety of hydrocarbon mixtures, even if the relative amount of different species is constrained by the property requirements. Recent research on surrogate mixtures were reviewed by Pitz and Mueller [1] starting with binary mixtures and then moving to more complex mixtures. For reproducibility reasons and for well-controlled modeling and experimental studies, it is useful to carefully select fixed chemical compositions of defined mixtures of reference species. Because fewer fuel compounds are involved, surrogates provide a cleaner basis for developing and testing models of the fuel properties in practical combustors. The use of a fixed surrogate also provides the basis for repeatable experimental studies. Variability in compositions of alternative transportation fuels reflects the use of different surrogates of each type of fuel. For example, gasoline surrogates typically contains C_6–C_9 components, biodiesel fuel surrogates are represented by mixtures of reference methyl esters, whereas a surrogate for oil sand fuels would contain higher amount of reference cycloalkane components. The technique of defining and using surrogate mixtures for transportation fuels is still in the early stages of development, and advances and refinements are always needed [3].

Table I schematically summarizes some major properties of transportation fuels. Ethanol, butanol, short-chain alcohols, together with fatty alcohols and fatty acid methyl esters (FAME) are potentially advanced biofuels, mainly useful as additive to fossil fuels. In fact, recent progress in metabolic engineering, and synthetic and systems biology, allowed the engineering of microbes to produce advanced biofuels with similar properties to petroleum-based fuels [10].

Before analyzing the chemistry and the oxidation mechanisms of the fuels, major properties of the different transportation fuels are shortly summarized in this paragraph.

Gasoline

Naphthas are complex mixtures directly obtained from crude distillation in a refinery. These streams, constituting 10–25 vol% of the crude oil, are generally characterized by specific gravity and distillation curves (ASTM D86 or TBP curves). Gasolines are produced by blending naphthas and different refinery streams

Table I Physical and Combustion Properties of Transportation Fuels

Fuel	Gasoline	Jet Fuel	Diesel	Ethanol	1-Butanol	Biodiesel
Specific gravity at 15°C	0.72–0.78	0.77–0.83	0.83–0.85	0.79	0.81	0.86–0.90
Boiling point range (°C)	30–220	150–300	200–350	78	118	260–360
Flash point (°C)	–43	38	52–60	13	35	140–170
Autoignition temperature (°C)	370	230	254	423	343	–
Research octane number (RON)	91–100	–	–	109	96	–
Motor octane number (MON)	82–92	–	–	90	78	–
Cetane number (CN)	<15	–	45–55	<15	25	55
Lower heating value (MJ/kg)	42–44	43–44	43–45	27	34	37

to meet the required performance specifications. Thus, gasoline composition varies widely, depending on the crude type, the process conditions, the season, and the product demand and specifications. Gasolines are volatile mixtures of practically all the hydrocarbons in the C_4–C_{12} fraction, distilling between ~30 and 220°C. Oil companies seasonally vary the initial cut to correspond to the weather conditions. In winter conditions, when only a small portion of the fuel is evaporated, the low-temperature end of the curve is a very important property. Many gasolines also contain blending components of a nonpetroleum origin, especially oxygenates such as ethers and alcohols.

Only two primary reference fuels (PRF), *n*-heptane and isooctane (2,2,4-trimethyl pentane), were and are commonly used to define a surrogate mixture and the octane reference scale, useful to represent the knocking propensity of real gasolines. The octane number (ON) is defined as 0 for *n*-heptane and 100 for isooctane. Research octane number (RON) and the motor octane number (MON) are determined in standard engine conditions following the ASTM (American Society for Testing and Materials) specifications. Standard pump gasoline can have a RON of 97 and a MON of only 87. The gasoline sensitivity, that is the difference between RON and MON, clearly indicates the limits of this simple surrogate formulation [11]. For these reasons, it is commonly accepted to extend the surrogate mixture, including also aromatic species. Thus, Gauthier et al. [12] and Davidson et al. [13] studied the ignition delay times of surrogate fuel mixtures of *n*-heptane, isooctane, and toluene. For the same reasons, Naik et al. [14] suggested to use, together with *n*-heptane, isooctane, and toluene, also methylcyclohexane to represent the cycloalkanes, and 1-pentene to represent the alkenes. Further attention to the kinetics of gasoline surrogates was also devoted by Mehl et al. [15], who suggested to include also 1-hexene.

Kerosene and Jet Propellant Fuels

Always depending on crude source and the refinery process, kerosene is a complex mixture in the C_9–C_{15} fraction with a distillation range 140–300°C. Kerosene-type jet fuels are relatively nonvolatile, and the major components are linear and branched alkanes (35%–50%), cycloalkanes (30%–35%), and one and two-ring aromatics (20% to 25 vol%). Jet fuels are blends of kerosene streams, sometimes supplemented with naphthas and low concentrations of additives to improve stability and performance. All jet fuels must be free of water and must be pumpable at very low temperatures and stable at higher temperatures. Common aviation fuels, used both for commercial and military aircraft, include Jet A, Jet A-1, and JP-8. U.S. Air Force military fuel (JP-8) is manufactured according to stringent military specifications. The pioneering works of Lindstedt and Maurice [16] and Edwards and Maurice [8] first analyzed several surrogate mixtures to mimic the properties of aviation fuels, both for experimental and computational tractability and reproducibility. Table II reports different surrogate mixtures proposed for JP-8 and aviation fuels by several researchers [17], specifically designed to reproduce different properties. Thus the Utah surrogate [9] was selected to reproduce the volatility of the fuel, whereas the Drexel [18] and San Diego surrogates [19] were designed to mimic fuel autoignition and flame extinction limits, respectively. Saffaripour et al. [20] used a three-component surrogate mixture of a Jet A-1 (69% *n*-decane, 11% *n*-propylcyclohexane, and 20% *n*-propylbenzene, on mole basis) to study soot formation in a laminar coflow diffusion flame. Eddings et al. [21] analyzed a series of six-component surrogates for the simulation of JP-8 burning rate in pool fires. Particular attention was devoted to the sooting tendency under pool fire conditions, highlighting the difficulties in the formulation of surrogates able to reproduce the fuel behavior over the lifetime of a batch pool fire.

Other surrogate mixtures were proposed by Montgomery et al. [22], Riesmeier et al. [23], and Honnet et al. [24]. Furthermore, Dooley et al. [25] studied and formulated a three-component surrogate fuel for a commercial jet fuel by constraining a mixture of *n*-decane, isooctane, and toluene to reproduce the average molecular weight (MW), the hydrogen on carbon ratio (H/C), the threshold sooting index (TSI), and the derived cetane number (DCN) of the target fuel. Moreover, Dooley et al. [26] formulated a quaternary surrogate mixture of *n*-dodecane/isooctane/1,3,5-trimethylbenzene/*n*-propylbenzene in a predictive manner to reproduce the same gas-phase combustion phenomena of POSF 4658. Jet-A POSF 4658 is a blend of five U.S. Jet A fuels from different manufacturers, which was analyzed by Widegren and Bruno [27] and extensively used by Dooley et al. [26]. A mixture of *n*-dodecane/isooctane/1,3,5-trimethylbenzene /n-propylbenzene of 40.4/29.5/7.3/22.8 mol% was selected as the "second-generation (POSF 4658) surrogate." This surrogate mixture was predicted to have a DCN of 47.1, a TSI of 21.4, a H/C of 1.96 and an average molecular weight of 138.7 g/mol.

Diesel Fuels

Gas oils are primarily used in the production of fuels for both industrial and domestic heating and for diesel engines. Also, gas oils are complex and variable

Table II Surrogate Mixtures for JP-8 and Aviation Fuels (mol%)

	Surrogate Components	Agosta [18]	Montgomery [22]	Violi [9]	Eddings [21]	Humer [19]	Humer [19]	Honnet [24]	Dooley [25]	Dooley [26]
Normal alkanes	*n*-Octane				3.7					
	n-Decane		29.9					77	42.7	
	n-Dodecane	22.9	28.4	23.2	31.7	46.0	44.3			40.4
	n-Tetradecane			12.9						
	n-Hexadecane				2.9					
Branched-alkanes	Isooctane			10.2					33.0	29.5
	Isocetane	24.2								
Cycloalkanes	Methylcyclohexane	21.1	23.4	26.5		27.7	30.4			
	Decalin	7.5			39.3					
Aromatics	Toluene						25.3		24.3	
	Xylene			21.0	12.2	26.3				
	1,2,4-TMB							23		7.3
	n-Propylbenzene									22.8
	Butyl-benzene		18.3							
	1-Methyl-naphthalene	24.3								
	tetralin			6.2	10.2					
Average molecular weight		159.2	138.3	133.0	145.3	133.2	128.4	137.2	120.7	138.7
H/C ratio		1.82	2.01	1.91	1.85	1.93	1.93	2.02	2.01	1.96

mixtures of hydrocarbons, predominantly C_{10}–C_{25} with boiling temperatures in the range of 150–450°C. Again, the chemical composition is dependent on the nature of the crude and on the refinery processes. The use of heavier atmospheric, vacuum, or cracked gas oil components is likely to result in an increase in the content of PAHs, some of which are known to be carcinogenic. Gas oils must meet specifications based on technical performance requirements, defined primarily in terms of physical properties. The diesel-range molecules produced from distillation of crude oil include paraffins, cycloparaffins, and aromatic molecules. The composition of diesel fuel is highly variable: The average carbon number is 14–15; the branched-alkanes are usually limited to one or two side methyl groups. The cycloalkanes typically have one ring with multiple alkyl side chains. Aromatics, which constitute 20–40% of commercial diesel fuels, are primarily one-ring, with some substituted two-ring aromatics [1]. Typical combustion property targets of diesel fuels include the threshold sooting index, the cetane number (CN), the fuel average molecular weight, and H/C ratio.

Two reference fuels can be used to define CN, which represents the time delay between the start of injection process and the fuel ignition as measured in internal combustion engines with ASTM specifications. In fact, CN is determined by the volume% of *n*-hexadecane ($C_{16}H_{34}$) in an isocetane (2,2,4,4,6,8,8-heptamethylnonane) mixture that provides the identical ignition delay of the measured fuel sample. *n*-Hexadecane ignites easily under compression and has a reference CN of 100, whereas isocetane has a CN of 15. α-Methylnaphthalene was previously used as the lower reference for diesel fuels, with a CN of zero. CN of normal diesel fuels are rated between 45 and 55. A higher cetane number means a shorter ignition delay time and rates the combustion propensity of diesel fuel, whereas the ON rates the ignition stability of gasoline.

The choice of surrogate mixtures is restricted by the availability of reference species inside validated chemical kinetic mechanisms [28]. Lin and Tavlarides [29] recently reviewed different surrogates of diesel fuels for representing thermophysical properties, including critical point, density, heat capacity, viscosity, and thermal conductivity. Single-component surrogates typically refer to *n*-alkanes, because they are major components of diesel fuels and their oxidation mechanisms are available and well established. *n*-Heptane was widely used as a surrogate because it has a similar cetane number as European diesel fuels [30,31] and because the kinetic mechanisms are relatively small and reliable. *n*-Hexadecane is also of great interest due to its molecular weight close to the one of diesel fuels. However, similarly to ON, CN alone is not representative enough for the ignition characteristics of diesel fuel at all engine conditions [28]; therefore, more complex surrogates were developed to include aromatic and naphthenic species, which are both important components of conventional diesel fuels [32].

Table III Surrogate Mixtures for Diesel Fuels (mol%)

	Surrogate Components	Gustavsson and Golovitchev [142]	Hernandez [143]	Xiao [28]	Hentschel [144], Barths [145]	Lemaire [146]	Seshadri [147]	Li [148]	Ra and Reitz [149]
Normal alkanes	*n*-Heptane	63.3	47.9	77.8					
	n-Decane				63.1	74.5	59.7	82.2	6.9
	n-Dodecane								21.4
	n-Tetradecane								22.9
	n-Hexadecane (CN = 100)								12.8
	n-Octadecane								10.8
Branched-Alkanes	Isocetane (CN = 15)								
Cycloalkanes	Cyclohexane			11.6					7.7
	Decalin								8.1
Aromatics	Toluene	36.7	52.1	10.6					9.5
	Xylene						40.3	17.8	
	1-MeNaphthalene (CN = 0)				36.9	25.5			
Average molecular weight		97.2	96.0	97.5	142.3	142.3	127.8	205.1	174.3
H/C ratio		1.82	2.01	1.96	1.92	1.93	1.93	2.02	2.01

Cycloalkanes and especially aromatics play an important role in soot formation. Owing to the rising interest in oil sands and shale oil, which have higher cycloalkane contents than conventional crude oil sources; the role of cycloalkane is also emphasized [28]. The surrogates of fuels for advanced combustion engines [33] were developed by modeling their distillation profiles. These surrogates were found to be able to represent real fuel properties including particularly, specific gravity, lower heating value, and distillation temperatures. Several of these surrogate fuels contain species which can be modeled by the POLIMI kinetic mechanism and are shown in Table III.

Biofuels and Biodiesel

As already observed, there is a growing interest in better studying and understanding alternate ways to obtain liquid fuels from nonfossil sources [10,34]. Biofuels are made by thermal, chemical, or biochemical biomass conversion, and they can result in solid, liquid, or gas form. There are two major liquid transportation fuels that might replace gasoline and diesel fuel: bioethanol and biodiesel, respectively [35]. Moreover, although challenges remain for commercial application, efficient processes are studied to first produce fructose from glucose, thus opening new paths for the production of 2,5-dimethylfuran as a further biomass-derived liquid transportation fuel [36].

Ethanol. Bioethanol is made by fermentation, mostly from carbohydrates produced in sugar or starch crops, such as corn or sugarcane. Cellulosic biomass, derived from nonfood sources, such as trees and grasses, is also a convenient and promising feed for ethanol production. Ethanol is widely used in the United States as a gasoline additive to increase ON and improve vehicle emissions, and also as a fuel in its pure form in Brazil. Ethanol, the only renewable liquid fuel currently produced in large quantities, suffers from several limitations, including low energy density, high volatility, and contamination by the absorption of water from the atmosphere [36]. Above all, its production is often in completion with food crops, thus contributing to higher food prices.

Butanol. In recent years, also the production of butanol and its use as a transportation fuel have become an interesting option, due to the significant increase of productivity and yields in the ABE (acetone–butanol–ethanol) fermentation process [37]. The octane rating of *n*-butanol is similar to that of gasoline but lower than that of ethanol and methanol. *n*-Butanol has a RON of 96 and a MON of 78, whereas t-butanol has octane ratings of 105 RON and 89 MON. t-Butanol is used as an additive in gasoline but cannot be used as a fuel in its pure form because its high melting point of 25.5°C causes it to freeze at room temperature. The fuel in an engine has to vaporize before to burn. Insufficient vaporization is a known problem with alcohol fuels during cold starts in cold weather. As the heat of vaporization of butanol is less than half of that of ethanol, an engine running on butanol should be easier to start in cold weather than one running on ethanol. Nowadays, biobutanol can be blended up to 10–12% in gasoline; vehicles are not able to use pure butanol.

Dimethyl-Ether. Dimethyl-ether (DME) is primarily produced by converting fossil sources or

lignocellulosic biomass (BioDME) via gasification to synthesis gas (syngas). Syngas is then catalytically converted into methanol, with subsequent methanol dehydration. DME is an interesting fuel in diesel engines, and gas turbines owing to its high cetane number, which is 55. Only moderate modifications are needed to convert a diesel engine to burn DME. DME is a good diesel fuel, with a low ignition delay and good combustion performances, without relevant soot formation. On the contrary, DME needs a lubricity improver and has a low calorific power due to the high oxygen content [38].

Biodiesel. Biodiesel refers to a vegetable oil- or animal fat-based diesel fuel consisting of long-chain alkyl esters. Biodiesel is typically made by chemically reacting lipids with an alcohol producing fatty acid alkyl esters. The transesterification process with methanol produces FAME, and glycerol is the side product. FAME has a lower energy content than diesel with a calorific value of about 37 MJ/kg. Biodiesel is slightly miscible with water and has a high boiling point and low vapor pressure. Rapeseed methyl ester (RME) in Europe and soybean methyl ester in the United States are the most common biodiesel fuels. They can be used alone, or blended with diesel in any proportions. Five major methyl esters (methyl palmitate, methyl stearate, methyl oleate, methyl linoleate, and methyl linolenate) are able to properly characterize these biodiesel fuels [39].

The hydrocracking or hydrogenation of vegetable oils can be used for the production of a renewable diesel fuel (green diesel), together with gasoline and propane. Recently, Luning-Prak et al. [40] studied several surrogate mixtures for representing the chemical composition and physical properties of an algal-based hydrotreated renewable diesel (HRD) fuel, and they concluded that the best surrogate is a simple mixture of linear and branched alkanes. Moreover, Gowdagiri et al. [41] analyzed the different ignition delay times of a conventional petroleum-derived military diesel fuel, and an alternative renewable diesel fuel derived from hydroprocessing algal oils. While the original fuel contains cycloalkanes, aromatics, and other compounds, HRD-76 is wholly composed of normal and lightly branched alkanes.

COMPLEXITY OF THE KINETIC MECHANISMS: LUMPING PROCEDURES AND REDUCTION TECHNIQUES

As already discussed, detailed kinetic mechanisms of liquid fuels are very complex and typically consist of a large number of species and reactions, even for pure components. Figure 1 shows the size of several detailed and lumped mechanisms of hydrocarbon and oxygenated fuels. There is a clear correlation between the number of species and reactions; similarly, these numbers increase with the size of the molecule, roughly in an exponential trend. Thus, the mechanism for *n*-decane (LLNL_nC10) involves 940 chemical species in 3878 elementary reversible reactions, whereas *n*-hexadecane mechanism (LLNL_nC16) includes 8130 reactions and 2116 species [42]. The Orléans detailed kinetics of biodiesel fuels is of similar sizes [43]. JetSurF is an oxidation mechanism specifically developed for aviation fuels up to *n*-dodecane and heavy alkylcycloalkanes limited to the high-temperature conditions; for this reason, it refers to less than 350 species [44]. Detailed kinetic mechanisms for heavy methyl esters (LLNL_Biofuels) may reach the order of about 5000 species [39]. Mechanisms of such sizes are even difficult to apply in 1D flame simulations [45]. Moreover, they have a wide range of different timescales resulting in computationally stiff problems. Therefore, the need to reduce the size and stiffness of the mechanisms, without significant loss in model predictions, is a well-defined target to make them practicable in multidimensional reacting flow simulations.

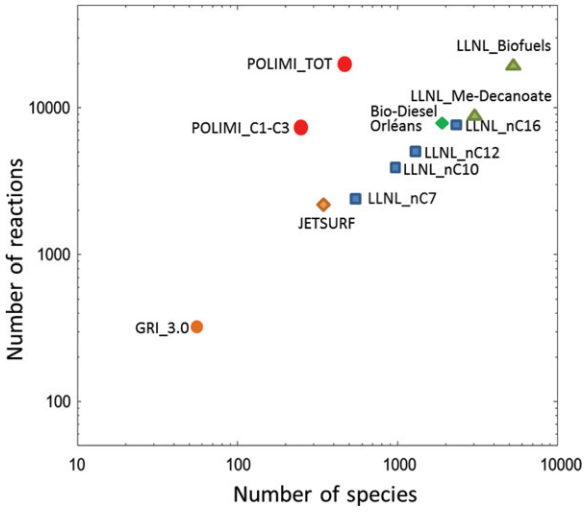

Figure 1 Number of reactions and species of selected detailed and lumped mechanisms for hydrocarbon and oxygenated fuels. After [45].

As already observed by McIlroy et al. [46] and further confirmed by Pitz and Mueller [1], while reaction mechanism reduction techniques have received considerable attention in recent years, better methods and more advance on automatic mechanism reduction are still needed, particularly for the large fuel molecules

that are characteristic of transportation fuels. Existing mechanism reduction tools are not always easy to use and not generally available. There are many ways to reduce the computational costs of including detailed fuel chemistry in reacting flow models. The first way is to reduce the number of species and reactions, while maintaining the accuracy required for a given application. This reduction can be done by lumping of species and by progressively reducing the kinetic scheme to a skeletal mechanism [1,47]. Further reduction techniques involve using a combination of chemical lumping, graphical reaction flow analysis, elimination methods, and a tailored optimization of specific reactions [48]. An alternative to reduce the size of the detailed mechanism is to save computational time by precalculating the chemistry and using lookup tables. Mechanism reduction can be done "on the fly" during a reacting flow calculation, so that much smaller mechanisms can be used at different times and locations on the computational grid. There are other ways to reduce computational times. For example, the computational efficiency of chemistry solvers can be improved, the chemistry can be solved on a coarser computational grid than the flow dynamics, as done in multizone HCCI engine calculations [1].

Lumping Procedures

Pyrolysis, partial oxidation, and combustion of heavy hydrocarbon fuels is a complex chain radical process involving a large number of reactions with several intermediate radical and molecular species. This is true for pure components, and it becomes obviously more evident for the complex mixtures of liquid transportation fuels. Since the pioneering work of Westbrook et al. [49], who proposed the first detailed low- and high-temperature oxidation mechanism of *n*-heptane, several detailed oxidation mechanisms have been developed for this component. The low-temperature chain radical oxidation mechanism, with the formation of extremely reactive hydroperoxide species, was identified and commonly accepted [16,50–53]. Large *n*-alkanes display the same kinetic behavior of *n*-heptane in both the high- and the low-temperature regions, and this similarity allows a direct extension of the overall kinetic model to species up to *n*-hexadecane [42,54]. Recently, further experimental studies of the low-temperature oxidation of *n*-alkanes in a jet-stirred reactor were performed. Through gas chromatography and synchrotron vacuum ultraviolet photoionization mass spectrometry, the different isomers of ketohydroperoxides and their decomposition products were identified and quantified [55].

As already discussed elsewhere [54], the low- and high-temperature oxidation mechanism of *n*-alkanes is at least based on 10 different classes of primary propagation reactions of alkyl radicals ($R^\bullet$):

R_1: isomerization of alkyl radicals;
R_2: β-decomposition of alkyl radicals;
R_3: O_2 H-abstraction to form $HO_2^\bullet$ and a conjugate alkene;
R_4: O_2 addition on $R^\bullet$ to form peroxy radicals ($ROO^\bullet$);
R_5: internal isomerization between $ROO^\bullet$ and hydroperoxyalkyl radicals ($^\bullet QOOH$);
R_6: decomposition of $^\bullet QOOH$ radicals to form small alkenes and aldehydes;
R_7: decomposition of $^\bullet QOOH$ radicals to form $HO_2^\bullet$ and conjugate alkenes;
R_8: decomposition of $^\bullet QOOH$ to form O-etherocycles and $OH^\bullet$;
R_9: O2 addition on $^\bullet QOOH$ to form hydroperoxyalkyl peroxy radicals ($^\bullet OOQOOH$);
R_10: decomposition of $^\bullet OOQOOH$ radicals to form ketohydroperoxides (OQOOH).

With reference to POLIMI kinetic mechanisms [54], Table IV reports some details of the oxidation mechanism of large *n*-alkanes in terms of the total number of reactions, primary propagation radicals, and intermediate species maintaining the same C number of the fuel. There are 362 primary propagation reactions of *n*-hexadecane, involving 100 different radicals (8 alkyl, 8 peroxyl, 42 hydroperoxyalkyl, and 42 hydroperoxyalkylperoxy) and 80 primary species always retaining 16 C atoms: 8 alkenes, 22 cyclic ethers, 8 hydroperoxides, and 42 carbonyl-hydroperoxides. The detailed description of successive reactions of all these new intermediate species rapidly makes overall detailed mechanisms scarcely manageable. As already mentioned, the mechanism for *n*-hexadecane includes more than 2000 chemical species and this total increases when additional submechanisms to characterize NO*x* or PAH and soot are added [42].

More complex radical mechanisms belong to the biodiesel fuels. A detailed chemical kinetic reaction mechanism for the five major components of soy biodiesel and rapeseed biodiesel fuels (methyl stearate, methyl oleate, methyl linoleate, methyl linolenate, and methyl palmitate) was developed by Westbrook et al. [39]. Low- and high-temperature mechanisms of large methyl ester molecules refer to the same reaction classes already identified in the previous kinetic scheme of *n*-alkanes. The presence of a methyl ester group in all of these fuel molecules and the presence of C=C double bonds in some of them modifies the types of reaction classes and the rates of specific

Table IV Number of Primary Propagation Reactions, Primary Radicals, and Primary Products Involved in the Detailed Oxidation Mechanism of Large *n*-Alkanes

	Reaction Class	*n*-C_7H_{16}	*n*-$C_{10}H_{22}$	*n*-$C_{12}H_{26}$	*n*-$C_{14}H_{30}$	*n*-$C_{16}H_{34}$
R_1	$R^\bullet \leftrightarrow R'^\bullet$	10	18	24	30	36
R_2	$R^\bullet \rightarrow R'^\bullet$ + alkene	5	8	10	12	14
R_3	$R^\bullet + O_2 \rightarrow C_nH_{2n} + HO_2^\bullet$	6	9	11	13	15
R_4	$R^\bullet + O_2 \leftrightarrow ROO^\bullet$	8	10	12	14	16
R_5	$ROO^\bullet \leftrightarrow QOOH^\bullet$	33	48	60	72	84
R_6	$QOOH^\bullet \rightarrow$ alkene + aldehyde + $OH^\bullet$	5	8	10	12	14
R_7	$QOOH^\bullet \rightarrow C_nH_{2n} + HO_2^\bullet$	6	9	11	13	15
R_8	$QOOH^\bullet \rightarrow$ cyclic ether + $OH^\bullet$	15	24	30	36	42
R_9	$QOOH^\bullet + O_2 \leftrightarrow {}^\bullet OOQOOH$	30	48	60	72	84
R_10	${}^\bullet OOQOOH \rightarrow OQOOH + OH^\bullet$	15	24	30	36	42
Total		135	206	258	310	362

	Primary Propagating Radical				Primary Product			
Fuel	$R^\bullet$	$ROO^\bullet$	${}^\bullet QOOH$	${}^\bullet OOQOOH$	Alkene	Cyclic-Ether	ROOH	Keto hydroperoxide
n-C_7H_{16}	4	4	15	15	3	8	4	15
n-$C_{10}H_{22}$	5	5	24	24	5	13	5	24
n-$C_{12}H_{26}$	6	6	30	30	6	16	6	30
n-$C_{14}H_{30}$	7	7	36	36	7	19	7	36
n-$C_{16}H_{34}$	8	8	42	42	8	22	8	42

reactions. Moreover, owing to the lack of symmetry in the structure, the detailed oxidation mechanisms of methyl esters involve a larger number of species and reactions. The resulting reaction mechanism contains more than 4800 chemical species and nearly 20,000 elementary chemical reactions (LLNL_Biofuels in Fig. 1). Similar sizes of the mechanisms are also found in the extensive research works on automatically generated detailed kinetic schemes for large *n*-alkanes [56,57] and for heavy methyl esters [58] with EXGAS code.

The kinetic modeling of large molecules benefits significantly from simplifications and semidetailed approaches. The main features of the chemical lumping approach adopted in pyrolysis and combustion systems were already reported and discussed elsewhere [50,59]. At high temperatures, the less favored interactions between large alkyl radicals and the reacting mixture allow a direct substitution of these radicals with their primary isomerization and decomposition products. Similarly, H-abstraction, addition on unsaturated bonds, and recombination reactions of heavy radicals are negligible with respect to their isomerization and decomposition reactions. All of the intermediate alkyl radicals higher than C4 can be then instantaneously transformed into their final and more stable products. On the basis of the steady-state approximation, continuity equations of heavy radicals allow to directly deduce the apparent stoichiometry of their decomposition path. Large sections of the detailed kinetic scheme can be reduced to a few equivalent or lumped reactions while still maintaining a high level of accuracy. Similarly, in the low-temperature mechanism, the lumped approach groups together not only the four classes of primary intermediate radicals but also all the isomers of the primary products (alkenes, cyclic ethers, and carbonyl hydroperoxides) [54]. Figure 2 schematically shows the lumped oxidation mechanism of *n*-dodecane, whereas Table V compares the number of primary propagation reactions and primary species for detailed and lumped kinetic schemes, always referring to POLIMI oxidation mechanisms [54]. Generally, the lumping of species smaller than C4 is not justified and these isomers are usually retained as individual species. The dimensions of the lumped kinetic scheme POLIMI_TOT, able to analyze the pyrolysis and combustion behavior of hydrocarbon and oxygenated fuels up to the reference species of diesel and biodiesel fuels, are shown in Fig. 1 and clearly highlight the advantages of the lumped approach: a significant reduction of the number of species, anyway conserving a high number of reactions.

Together with the *horizontal* lumping among isomer species, the lumping of homologous species with

Table V Comparison of Detailed and Lumped Kinetic Mechanisms of *n*-Dodecane and *n*-Hexadecane in Terms of Numbers of Primary Propagation Reactions and Primary Radicals and Products

	n-Dodecane		*n*-Hexadecane	
	Detailed kinetics	Lumped kinetics	Detailed kinetics	Lumped kinetics
Primary reactions	258	15	362	15
Intermediate radicals	72	4	100	4
Primary products	58	4	80	4
Alkenes	6	1	8	1
Hydroperoxides	6	1	8	1
Cyclic ethers	16	1	22	1
Ketohydroperoxides	30	1	42	1
Total	446	27	622	27

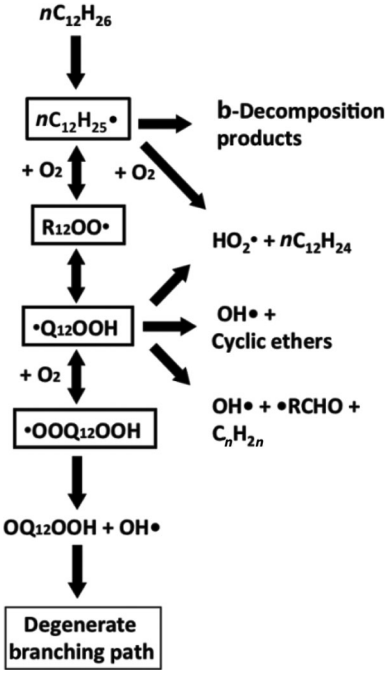

Figure 2 Lumped oxidation mechanism of *n*-dodecane.

a different number of carbon atoms can be conveniently adopted. Let us refer to this as *vertical* lumping, i.e., lumping of homologous species inside a family (such as *n*-alkanes, iso-alkanes, alkenes, methyl esters) with different molecular weights. The reactivity and the product distribution of large hydrocarbons with N_c carbon atoms can be correctly and conveniently estimated with a linear combination of the reactivity and product distribution of the homologous species with $(N_c - i)$ and $(N_c + j)$ carbon atoms, with i and j generally equal to 1–3. This *vertical* lumping allows to further reduce the number of species. Thus, instead of considering all the 10 *n*-alkanes from C_7 to C_{16}, only *n*-heptane, *n*-decane, *n*-dodecane, and *n*-hexadecane are included as pure and/or reference components in the POLIMI mechanism, with a clear advantage in terms of the number of species. Intermediate species are derived with the lever rule; thus a molar mixture *n*-heptane/*n*-decane 2/1 represents *n*-octane, whereas the mixture 1/2 mimics *n*-nonane. Similarly, *n*-tetradecane is represented as an equimolar mixture of *n*-dodecane and *n*-hexadecane.

Reduction Methods

As pointed out by Lu and Law [45], the current reduction methods rely on automatic simplifications of the original kinetic schemes. The unimportant reactions and species are identified by focusing on different parameters. For example, the reduction method of Wang and Frenklach [60] identifies the unimportant reactions by comparing the reaction rates with that of a properly chosen reference reaction. The method of directed relation graph (DRG), developed by Lu and Law [61], reduces the number of species by identifying their different couplings. Once a set of "important" species is identified upstream, the relative contribution of each of the remaining species of the detailed mechanism to the production rate of the important species is quantified: If and only if it is significant, these species are kept; otherwise, they are not considered in the reduced mechanism. In this way, the DRG method reduces the number of mass balance equations. Skeletal mechanisms discussed and reported in this work have been obtained with the reacting flux analysis (RFA), further complemented with a sensitivity analysis. The RFA reduction technique analyzes the behavior of the original mechanism in ideal, isothermal plug flow reactors, whose operating conditions are homogeneously spread over the range of operating conditions in terms of

temperature, pressure, residence time, and stoichiometry. In particular, the importance of each species is evaluated according to the production and consumption rates throughout the whole reactor. For each reactor, the absolute formation rate of each *i*th species is evaluated as

$$R_i = \sum_{j=1}^{NR} \left| v_{i,j} \omega_j \right| \quad (1)$$

where *NR* is the number of reactions, v_{ij} is the stoichiometric coefficient of the *i*th species in the *j*th reaction, and ω_j is the net reaction rate of the *j*th reaction. The total flux of each species in each reactor is evaluated as

$$F_i = \int_0^{t_f} R_i \, \mathrm{d}t \quad (2)$$

where t_f is the residence time of each reactor. Once normalized with respect to the local maximum value, a threshold is fixed to locally keep the required accuracy, and for each reactor a subset of important species is individuated. Then, the final mechanism is obtained as the union of all the subsets. On the other hand, the reactions are kept if and only if all the reactants and products belong to the final set of retained species. The presence of inert species is forced in the mechanism, even if their fluxes are null. Previous experiences on the reduction of *n*-dodecane oxidation mechanism [62] clearly showed that the skeletal mechanism obtained by reducing a lumped mechanism involved about 120 species, whereas about 300 species were required by the reduced mechanism derived from a detailed scheme [42]. This fact is further confirmed by the recent work of Narayanaswamy et al. [63], who reduced the detailed kinetics of *n*-dodecane to 295 species. When reducing a detailed mechanism, a successive lumping phase is always required. Lumping procedures allowed to further reduce the kinetic scheme from 295 to 188 species. The isomers of radical species important in the low-temperature region were grouped according to the size of the ring involved in the transition state of the corresponding isomerization reactions. A similar lumping was extended to other primary species in *n*-dodecane propagation, such as cyclic ether and ketohydroperoxide isomers. Figure 3 schematically summarizes this approach.

The dimensions of the reduced scheme derived from lumped mechanisms are smaller than the ones of the schemes derived from the detailed ones. The gray arrows highlight the major effect of the lumping, that is a significant reduction of the number of species, either directly obtained during the automatic generation of the whole kinetic scheme or applied to the reduced model derived from the detailed ones. The great advantage of a direct use of lumping procedures when generating the detailed kinetic schemes is a simpler and more effective validation phase already and directly accomplished on the lumped mechanism.

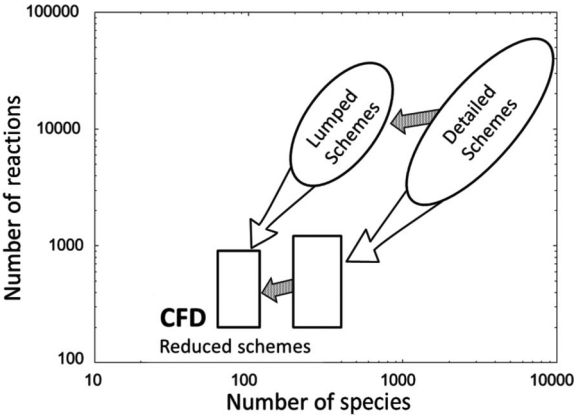

Figure 3 Strategies for the reduction of lumped and detailed kinetic schemes. Gray arrows represent the lumping phases.

SKELETAL KINETIC SCHEMES OF LIQUID TRANSPORTATION FUELS

All the skeletal mechanisms of the different liquid fuels here discussed are derived from the complete POLIMI_1404 kinetic scheme available, in Chemkin format with thermo and transport properties, in the CreckModeling Web site (http://creckmodeling.chem.polimi.it). Since the very pioneering work on the development of the kinetic scheme of hydrocarbon pyrolysis [64] and of oxidation of methane and C_2 species [65], the modular POLIMI mechanism was validated in a wide range of conditions for increasingly heavier species up to the gasoline primary reference fuels: *n*-heptane [66] and isooctane [67]. The successive kinetic studies on naphthenes [68,69], reference components of kerosene and aviation fuels [9,18,19,70], and heavier *n*-alkanes [54] allowed to extend the prediction capability of the overall kinetic model. The role of alkene combustion was then investigated, mainly in respect of ON and gasoline sensitivity [11,71]. The pyrolysis and oxidation mechanism of kerosene and jet fuels was further validated in reproducing different combustion targets, such as autoignition delay times, extinction and ignition limits in diffusion flames [72], and with attention to

Table VI Skeletal Mechanisms Discussed in This Work

Fuel	Mechanism	Reference Species	Name
Gasoline	*n*C7	*n*-Heptane	POLIMI_NC7_106
	Gasoline	*n*-Heptane, isooctane, toluene	POLIMI_GASOLINE_156
	Biogasoline	*n*-Heptane, isooctane, toluene, alcohols	POLIMI_BIOGASOLINE _171
Jet fuels	*n*C12	*n*-Decane and *n*-dodecane	POLIMI_NC12_130
	Kerosene	Heavy *n*-alkanes, isooctane, isocetane, methylcyclohexane, toluene, xylene, C9-aromatics, decaline, tetraline	POLIMI_KEROSENE_231
	HT_Kerosene	See kerosene	POLIMI_KEROSENE_121
Diesel	Diesel	*n*-Alkanes, iso-alkanes, toluene, xylene, methylnaphthalene	POLIMI_DIESEL_201
	BioDiesel	Fatty acid methyl esters	POLIMI_FAME_177
	Diesel-BioDiesel	*n*-Alkanes, aromatics, methylnaphthalene, heavy methyl esters	POLIMI_DIESEL_FAME_226

the main paths to benzene and PAH formation at high temperatures and sooting conditions [73]. More recently, the mechanism was extended to oxygenated and biomass derived fuels, such as alcohols [74–76], DME [77], light and heavy fatty acid methyl esters [78–80], and reference components of diesel fuels, such as decalin and tetralin [81–83]. Finally, a broad validation work on aromatics [84] as well as a comparative analysis of the laminar flame speeds of different fuels [85] further contributes to settle the reliability of the overall POLIMI kinetic model. Several examples are here reported to validate the different reduced models. These comparisons allow to further check the reliability of the complete kinetic model in respect of more recent experimental data. We will derive and discuss several skeletal mechanisms, which are named with the following format: *POLIMI_NAME_XX*, where *XX* is the number of species. Table VI summarizes the analyzed schemes.

All the reduced kinetic models are reported in the Supporting Information, together with the error maps of the ignition delay times. These maps show the error deviations between the complete and the reduced kinetic schemes. The common target is to maintain deviations below 15%, in the whole range of operating conditions. All the reduced models are also available, in Chemkin format with thermo and transport properties, in the CreckModeling Web site (http://creckmodeling.chem.polimi.it).

In this work, we limit our attention to the lumping procedures and to the first step useful to reduce the size of the original mechanism. To maintain the standard structure of the skeletal kinetic schemes, successive reduction phases, such as the timescale reductions with quasi-steady-state approximations for species and partial equilibrium approximation for reactions [86], are not considered. While the size of these kinetic models already allows detailed computational fluid dynamics (CFD) calculations in internal combustion engines [87], further reduction phases, usually tailored to specific and optimized solvers, are necessary when the interest is toward more complex CFD computations.

Table VII Operating Conditions Used to Generate the Skeletal Mechanisms

Condition	Range
Temperature	600–1700 K
Pressure	1– 40 atm
Equivalence ratio	0.5 – 2

Table VII describes, in terms of temperature, pressure, and equivalence ratio, the operating range of interest for the development and validation of the skeletal mechanisms. Scheme reduction is then performed referring to a set of ideal reactors, whose operating conditions are homogeneously spread over these ranges.

All simulations were performed with the OpenSMOKE code [88], with an extensive use of the BzzMath numerical library [89,90].

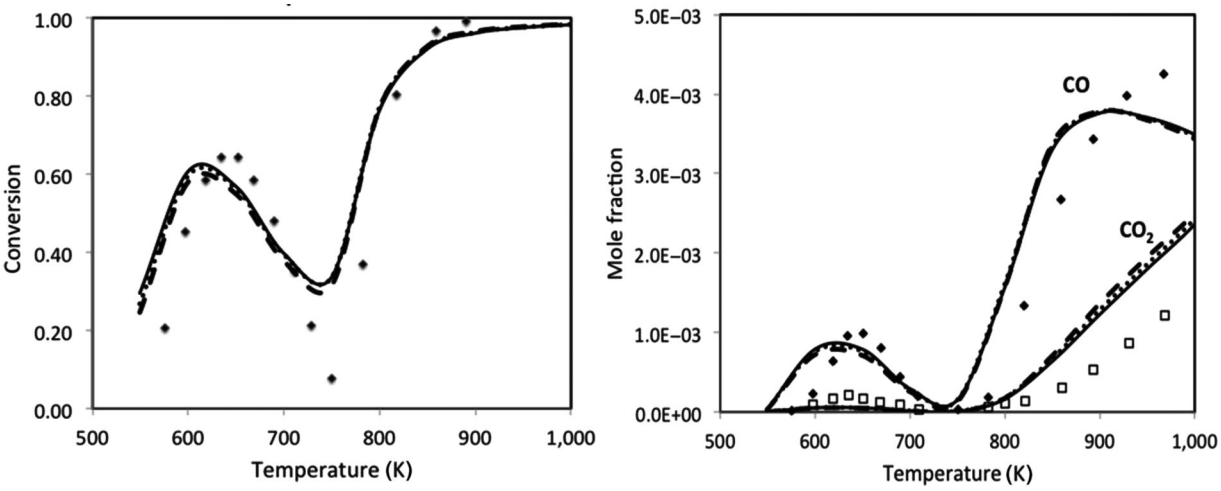

Figure 4 *n*-Heptane conversion and CO and CO_2 formation in a jet-stirred reactor [91]. Comparisons of experiments (symbols) and original (solid line) and reduced schemes (106 species: dotted lines; 90 species: dashed lines).

Skeletal Kinetic Schemes of Gasoline

Skeletal Kinetic Scheme of n-Heptane. Stagni et al. [62] already discussed and presented a reduced kinetic scheme for *n*-heptane oxidation, derived from the overall POLIMI kinetic scheme. The skeletal mechanism *POLIMI_NC7_106*, simply obtained by applying the RFA method, is constituted by 100 species and is reported in the Supporting Information. Figure 4 shows a comparison of the experimental and model predicted *n*-heptane conversion, CO and CO_2 formation in a jet-stirred reactor [91]. Model predictions refer to the complete model and to two different reduced models with 106 and 90 species, respectively. According to the required precision in the overall range of conditions, the reduced model with 106 species was chosen, even though they behave very similarly in this example.

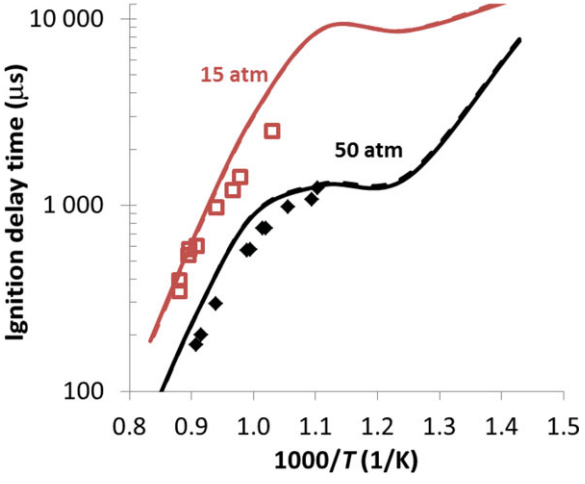

Figure 5 Ignition delay times of stoichiometric oxidation of a ternary *n*-heptane, isooctane, and toluene mixture surrogate of RD387 gasoline at 15 and 50 atm. Experimental (symbols) [12] and predictions of the original (solid line) and reduced scheme POLIMI_GASOLINE_156 (dashed lines).

A 290 species skeletal mechanism for *n*-heptane oxidation was derived by Saylam et al. [47] when reducing the 545 species of LLNL detailed mechanism [51], with a joint analysis of reaction rates and sensitivities. With the same accuracy, the skeletal model derived from a lumped scheme contains about one third of the species required by the skeletal model derived from the detailed mechanism, as already shown in Fig. 2 and further discussed by Stagni et al. [62].

Skeletal Kinetic Schemes of Ternary Gasoline Surrogate (n-Heptane–Isooctane–Toluene). Following the same reduction procedure, the skeletal mechanism POLIMI_GASOLINE_156 for a three-component surrogate mixtures involving *n*-heptane, isooctane, and toluene was derived. A ternary mixture *n*-heptane–isooctane, and toluene 63/20/17 by mole fraction was selected by Gauthier et al. [12] as a surrogate of RD387 gasoline. Figure 5 shows a comparison of the ignition delay times of the stoichiometric oxidation in air of a gasoline surrogate at 15 and 40 atm. The predictions of the skeletal and the original model overlap in all the conditions and reasonably agree with the experimental data.

Recently, Sileghem et al. [92] measured laminar burning velocities of neat isooctane, *n*-heptane, toluene, and a ternary mixture, as a surrogate of a commercial gasoline, at 298 and 358 K. By changing the

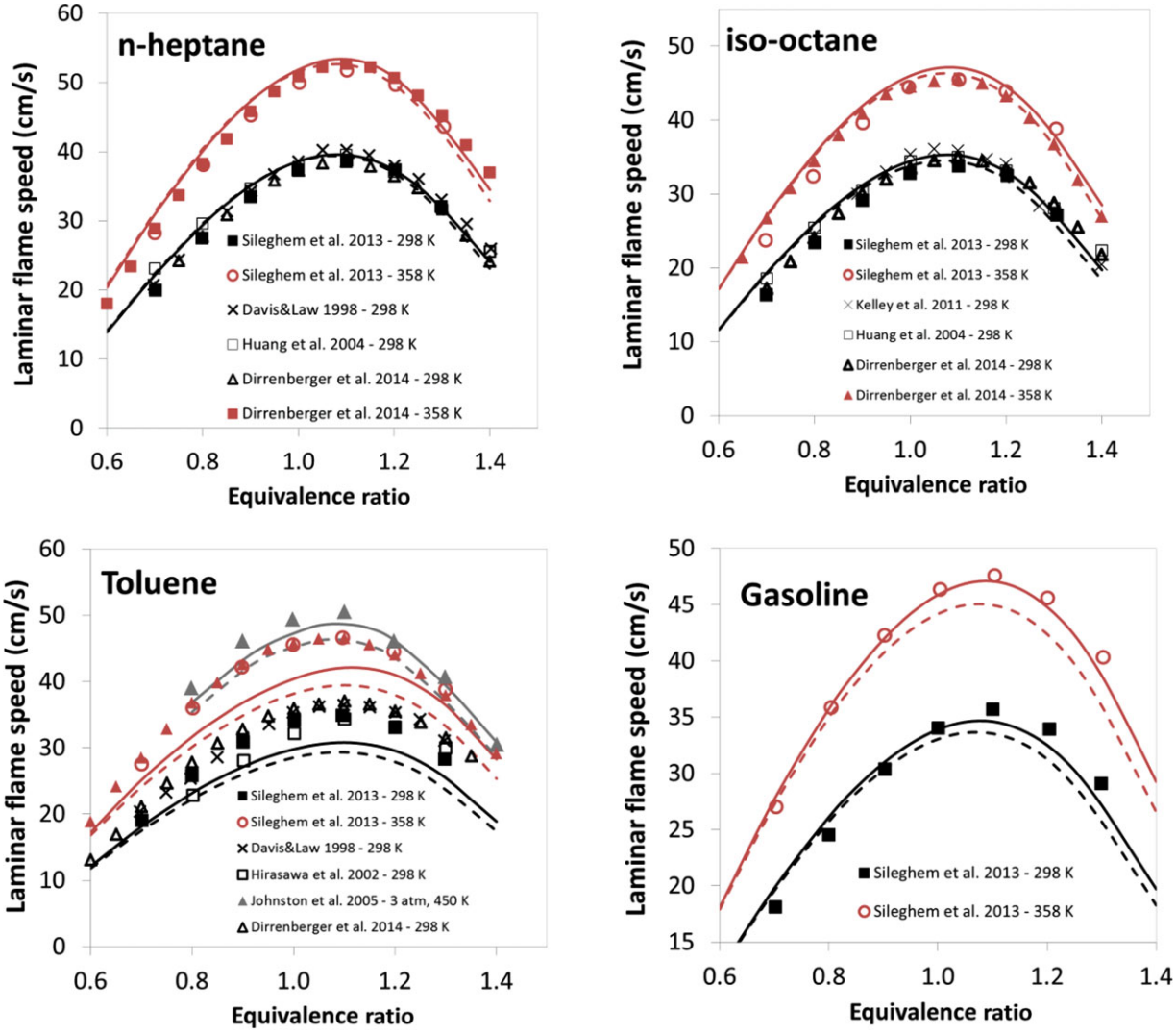

Figure 6 Laminar flame speed of isooctane, *n*-heptane, toluene, and a surrogate ternary mixture. Experimental (symbols); predictions of original (solid lines) and skeletal model POLIMI_GASOLINE_156 (dashed lines) [92,150–154].

fraction of the components in the mixing rule, they found that a mixture of 1/3 isooctane, 1/3 *n*-heptane, and 1/3 toluene on volume basis was a good surrogate of the commercial gasoline. Figure 6 shows a satisfactory comparison of experimental laminar flame speeds and the predictions of the original and the skeletal model, for the three reference fuels and for the ternary mixture. The skeletal mechanism almost completely overlaps with the detailed one, in these conditions. Minor deviations, in the order of 1–2 cm/s, are observed in rich conditions possibly due to the effect of removed radical recombination reactions, mainly in the case of toluene.

The detailed LLNL mechanisms of *n*-heptane (545 species) and isooctane (858 species) [51,93] were reduced by Saylam et al. [47] to a skeletal mechanism of about 500 species, again about three times more than the species required by the lumped derived skeletal mechanism. Moreover, this number of species is fully consistent with the size of the skeletal mechanism of *n*-heptane and isooctane derived by Luong et al. [94]. It is to be noted that these reduced models are able to reproduce not only autoignition delay times but also species concentration profiles versus temperature obtained in jet-stirred and flow reactors. Moving from the LLNL detailed kinetics of *n*-heptane and isooctane [51,93], Luong et al. first obtained a skeletal mechanism with 368 species and 1889 reactions. To reduce the mechanism size further, they applied a lumping method. Isomer lumping detects isomer groups, and the

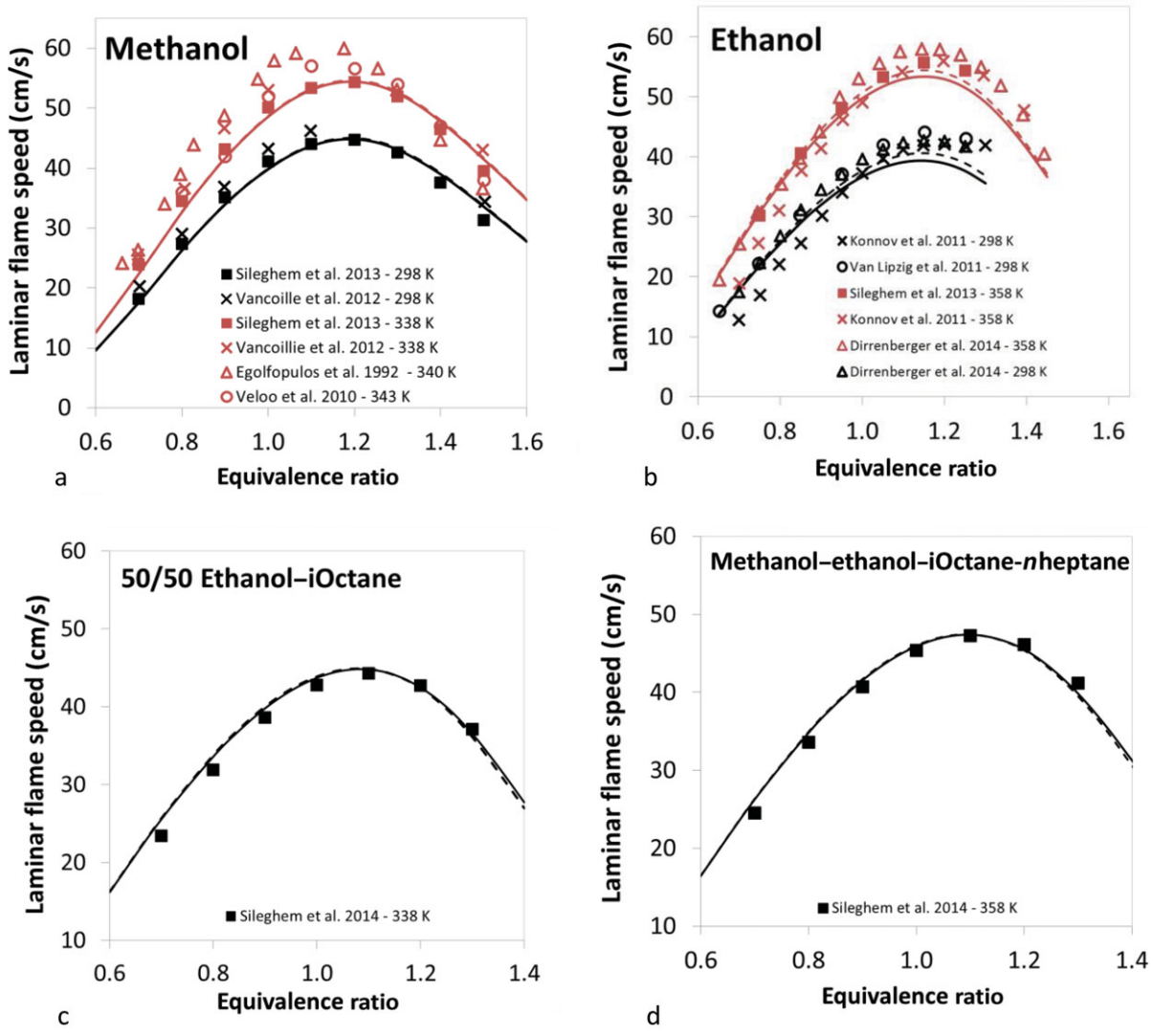

Figure 7 Laminar flame speeds of pure methanol and ethanol and biogasoline. (a) Methanol. (b) Ethanol. (c) Binary mixture ethanol and isooctane (50% v/v each). (d) Quaternary mixture of methanol, ethanol, isooctane, and *n*-heptane (25% v/v each). Experimental [92,95,155–160] (symbols); predictions of original (solid and dashed lines) and skeletal model POLIMI_BIOGASOLINE_171 (dotted lines).

group reaction rates are computed as a weighted sum of the reaction rate of each isomer. The DRG-aided sensitivity analysis method [45] was subsequently used, and a skeletal mechanism with 171 species and 861 reactions was finally obtained. This number of species well agrees with the 156 species of the skeletal mechanism POLIMI_Gasoline_156. Successive reduction techniques, mainly based on steady-state approximation and analytical solution of the associated reactions as well as eliminating chemical timescales shorter than 10 ns, allowed to obtain a 116-species skeletal mechanism for the oxidation of the two primary reference fuels [94].

Skeletal Kinetic Schemes of Biogasoline (n-Heptane–Isooctane–Toluene–Alcohols). The skeletal mechanism POLIMI_BIOGASOLINE_171 was derived by including simple alcohols, such as methanol, ethanol, and *n*-butanol, in the previous ternary mixture of *n*-heptane, isooctane, and toluene. Seven of the new species with respect to the previous gasoline skeletal mechanism belong to the mechanism of 1-butanol: Four alkyl radicals of 1-butanol and three peroxy lumped radicals are useful to describe the low-temperature reactions of 1-butanol. Both methanol and ethanol, with related radicals, were already considered in the previous skeletal mechanism of gasoline.

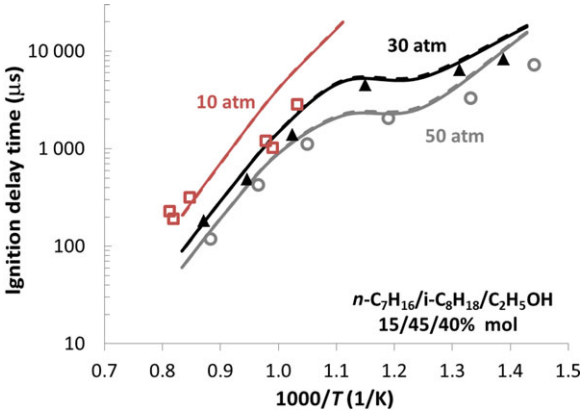

Figure 8 Ignition of nC$_7$H$_{16}$/iC$_8$H$_{18}$/C$_2$H$_5$OH air stoichiometric mixtures at different pressures. Comparison between experimental data (symbols) [96] and predictions of original (solid lines) and reduced model POLIMI_BIOGASOLINE_171 (dashed lines).

Laminar speeds of atmospheric flames of methanol, ethanol, and different mixtures of these with isooctane and *n*-heptane, were very recently measured by Sileghem et al. [95], at 298 and 358 K. Thus, Fig. 7 satisfactorily compares these new experimental measurements and predicted laminar flame speeds of pure methanol and ethanol, a binary mixture ethanol and isooctane (50% v/v each), and a quaternary mixture of methanol, ethanol, isooctane, and *n*-heptane (25% v/v each). Both models predict laminar flame speeds, within the experimental uncertainties.

The chemical interaction between ethanol and PRF were investigated by Fikri et al. [96] in a shock tube device. The ignition delay time of a stoichiometric mixture nC$_7$H$_{16}$/iC$_8$H$_{18}$/C$_2$H$_5$OH (18/62/20 liquid vol%, 14/46/40 mol%) was measured in a heated high-pressure shock tube in the temperature range 690–1200 K at pressures of 10, 30, and 50 atm. This fuel composition mimics an oxygenated gasoline with RON 95.1 and MON 89.5. Figure 8 shows the comparison between the experimental data and the predictions of the detailed and the reduced models. The temperature and pressure effects are correctly reproduced by both models. Ethanol is responsible for the disappearance of the negative-temperature-coefficient (NTC) region, favoring in this way the ignition propensity in the intermediate T region. On the contrary, the presence of ethanol increases the resistance to ignition in the low T region, where knock typically occurs. Of course, at high temperatures the promoting–inhibiting effect vanishes and gasoline and biogasoline behave similarly [74].

As a further example, a mixture of *n*-butanol and *n*-heptane (20/80 and 50/50 mol%) was studied in a jet-stirred reactor, in the temperature range 530–1070 K, at 10 atm, and with 750 ppm of initial fuel at three equivalence ratios (0.3, 0.5 and 1) [97,98]. Comparisons are limited to a 50/50 mixture of *n*-heptane and *n*-butanol at $\Phi = 0.3$. More detailed comparisons between model predictions and the whole set of experimental data are reported in Bissoli et al. [99]. Good agreement between the experimental results and the computations can be observed in Fig. 9. The model is able to reproduce the onset of the low-temperature reactivity, the NTC region, and the high-temperature ignition, which occurs at ~800 K. Moreover, the model is also able to predict the characteristic low-temperature intermediate species, such as CH_2O, CH_3CHO, and butanal. It is important to notice that under these conditions, the reactivity of the system is mainly controlled by the more reactive *n*-heptane, which is characterized by an intense low-temperature chemistry and a more pronounced NTC. Nevertheless, the butanol low-temperature mechanism plays a significant role [99]. Also in this case, it is possible to observe that the predictions of the reduced model POLIMI_Biogasoline_171 are very close to the ones of the complete kinetic scheme.

Skeletal Kinetic Scheme of Kerosene and Jet Fuels

Skeletal Kinetic Scheme of Kerosene and Jet Fuels (n-Decane and n-Dodecane). The skeletal mechanism of *n*-dodecane and lighter *n*-alkanes oxidation POLIMI_NC12_130 was derived, always with the same procedure and conditions. Figure 10 shows a comparison of experimental data with the predicted *n*-dodecane conversion, as well as CO and CO_2 formation in a jet-stirred reactor [100]. Model predictions refer to the original kinetic scheme and to the reduced one. As already mentioned, Narayanaswamy et al. [63] reduced the LLNL detailed kinetics of *n*-dodecane to 295 species, again more than the double of the species required by the skeletal mechanism POLIMI_NC12_130.

Skeletal Kinetic Schemes of Kerosene and Jet Fuels. The skeletal mechanism for kerosene and aviation fuels, POLIMI_KEROSENE_231, involving *n*- and isoalkanes, methylcyclohexane, aromatics (from toluene up to C9 aromatics), and finally decalin and tetralin, was derived with the same procedure. This model involves 231 species and is able to characterize most of the surrogate mixtures of Table II, including pure *n*-dodecane. The relative large number of species is due to the variety of reference components

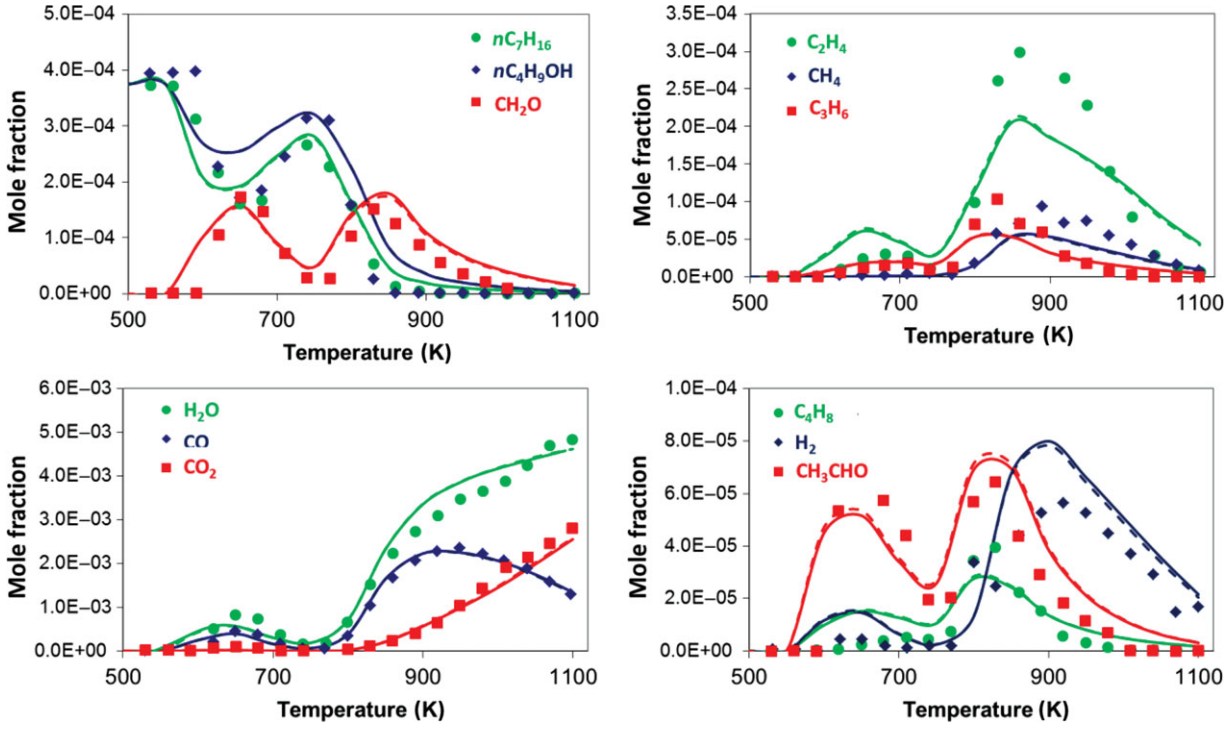

Figure 9 *n*-Butanol–heptane mixture (50:50) at $\Phi = 0.3$, $P = 10$ atm at and $\tau = 0.7$ s. Comparison between experimental data [98] and model predictions. Complete mechanism: continuous lines, Reduced mechanism POLIMI_BIOGASOLINE_171: dotted lines.

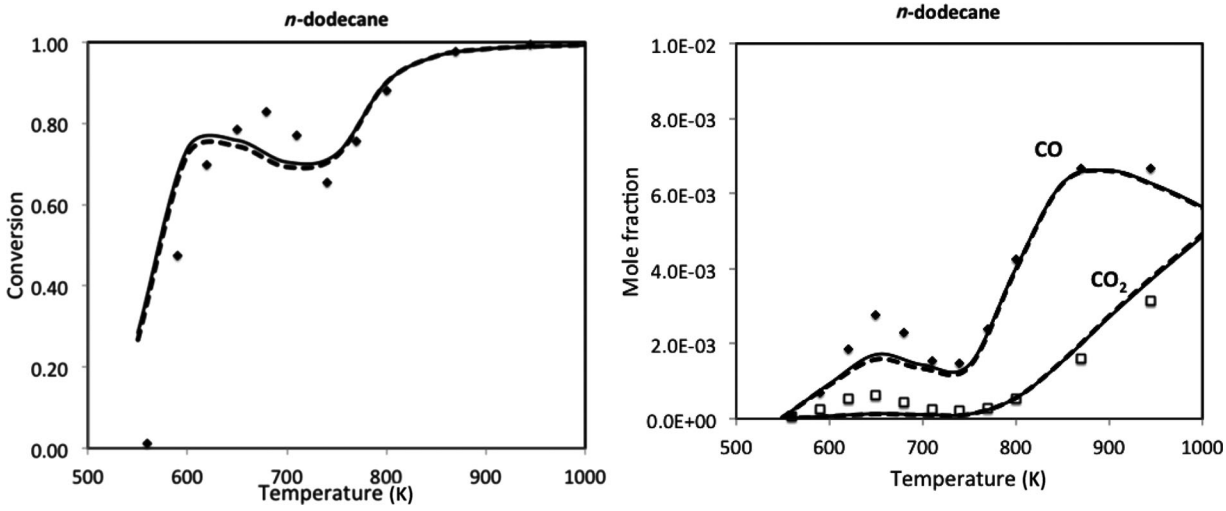

Figure 10 *n*-Dodecane conversion and CO and CO_2 formation in a jet-stirred reactor [100]. Comparisons of experiments (symbols) and original (solid lines) and reduced scheme POLIMI_NC12_130 (dashed lines).

of the different surrogate mixtures. Owing to the great interest of the high-temperature combustion of jet fuels, a further reduced scheme has been derived: POLIMI_HT_KEROSENE_121. The difference in the number of species clearly highlights the complexity of the low-temperature oxidation mechanism.

Figure 11 shows a further comparison for the ignition delay times and multispecies time histories, as measured by Davidson et al. [101] during *n*-dodecane oxidation in a shock tube, at 1410 K. These comparisons show the very similar predictions of the original model, the POLIMI_NC12_130 and the high-temperature skeletal model of kerosene with 121

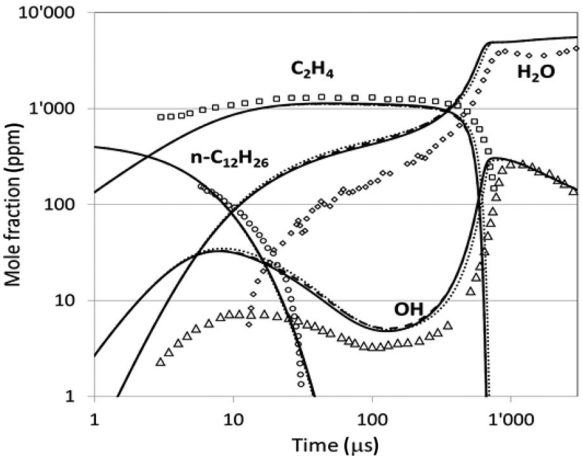

Figure 11 Time histories of radical and major species in *n*-dodecane oxidation at 1410 K, and 2.3 atm [101]. Comparisons of experimental data (symbols) with predictions of the original lumped model (solid lines), the skeletal POLIMI_NC12_130 (dashed lines), and the POLIMI_HT_Kerosene_130 model (dotted lines).

species. The time histories of *n*-dodecane and ethylene, as well as the one of OH radical, are properly kept by all the models in a very similar way.

As shown in Table II, C_9 aromatics are important components of real and surrogate jet fuels and they can produce a significant amount of benzyl-like resonantly stabilized radicals inhibiting in this way the mixture reactivity. Darcy et al. [102] recently studied the high-pressure *n*-propylbenzene ignition using a rapid compression machine. Moreover, the laminar flame speeds of two C_9H_{12} isomers, *n*-propylbenzene, and 1,3,5-trimethyl benzene were measured by Kim et al. [103] at atmospheric pressure and different equivalent ratios. Figure 12 compares experimental and predicted laminar flame speeds of the two isomers at 353 and 400 K. A single lumped trimethylbenzene component (TMB) is used in the POLIMI mechanism, without distinction among the different isomers. The flame speed of *n*-propylbenzene is nearly 8 cm/s higher than that of TMB. Owing to the very low bond dissociation energy [104], the cleavage of the C–C bond of *n*-propyl benzene to form benzyl ($C_6H_5CH_2$) and ethyl radical is a significant source of radicals for *n*-propylbenzene. On the contrary, the H abstractions on the methyl group of trimethylbenzene are highly favored, with the important formation of the resonantly stabilized C_9H_{11} radical. Both the original and the skeletal kinetic models agree each other and confirm these different flame speeds. The higher reactivity of *n*-propylbenzene with respect to toluene, xylenes, and trimethylbenzene is theoretically and experimentally confirmed [105,106]. Moreover, the POLIMI kinetic mechanism was further validated by comparing the laminar flame extinctions of xylene and trimethylbenzene with respect to those of *n*-alkanes and cycloalkanes [107].

Methylcyclohexane and decalin (bicyclic alkane component) are important reference species in surrogate mixtures of fossil transportation fuels, as shown in Table II. Recently, Comandini et al. [108] experimentally investigated the oxidation of cyclohexane and decalin by measuring shock tube ignition delay

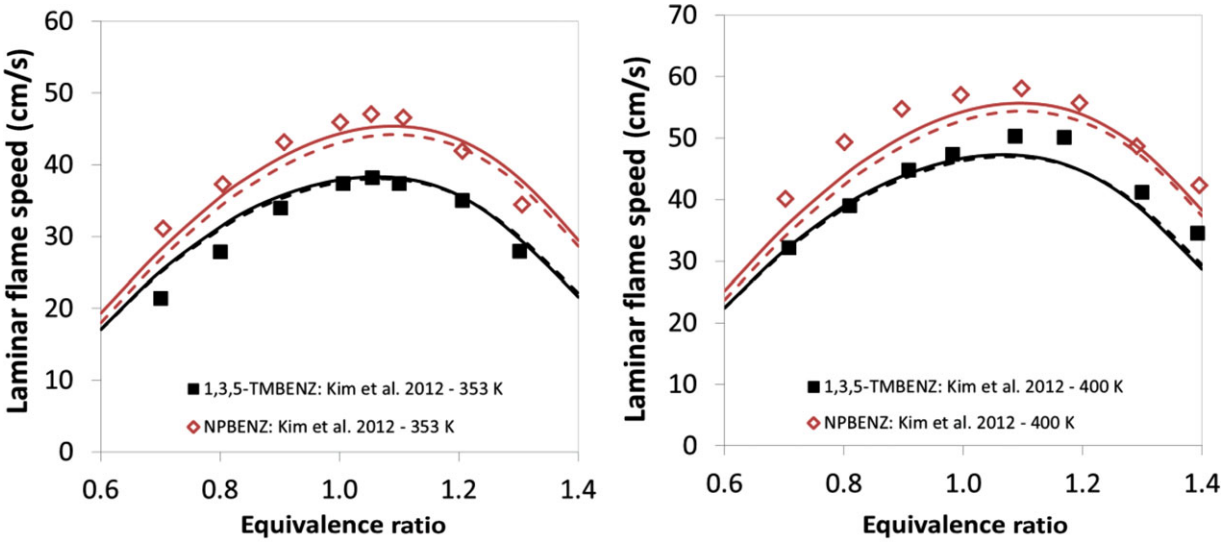

Figure 12 Laminar flame speeds of *n*-propylbenzene and 1,3,5-trimethylbenzene, at 353 and 400 K. Experimental (symbols) [103] and predictions of the original (solid lines) and skeletal model POLIMI_KEROSENE_HT_121 (dashed lines).

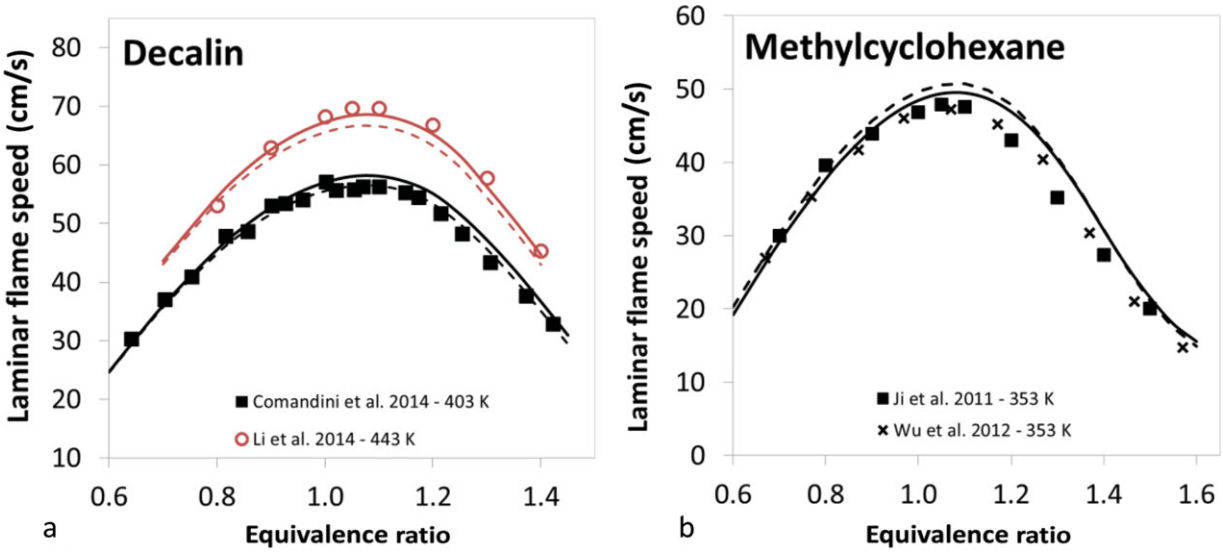

Figure 13 Laminar flame speeds of decalin (Panel a) and methylcyclohexane (Panel b). Experimental (symbols) [108–111] and predictions of the original (solid lines) and skeletal model POLIMI_KEROSENE_HT_121 (dashed lines).

times of highly diluted mixtures in argon and laminar flame speed in a spherical bomb. They observed that the autoignition process of the double-ring structure is slower compared to the single-ring case; similarly, the maximum flame speed for decalin is lower compared to the one of cyclohexane by ~10%. Laminar flame speeds of decalin air mixtures were also measured in the counterflow configuration at atmospheric pressure and 443 K by Li et al. [109]. Panel a of Fig. 13 shows a satisfactory comparison of model predictions with both sets of experimental data. As a matter of further comparisons, panel b of the same figure shows the laminar flame speed of methylcyclohexane [110,111].

Owing to the importance of decalin, ignition delay times and ethylene concentration time histories were recently measured by Zhu et al. [112] behind reflected shock waves during decalin oxidation and pyrolysis. High pressure ignition delay measurements at 769–1202 K, and different equivalence ratios allowed to observe a negative-temperature-coefficient (NTC) behavior. Figure 14 shows a satisfactory comparison of the experimental data with the predictions. Again the predictions of the original and skeletal models almost overlap in all the analyzed conditions.

A ternary molar surrogate of *n*-decane (82.1%), methylcyclohexane (7.9%), and toluene (10%), with a H/C ratio of 2.110, which is typical of most commercial jet fuels, was studied by Denman et al. [113], using particle image velocimetry in a stagnation flame

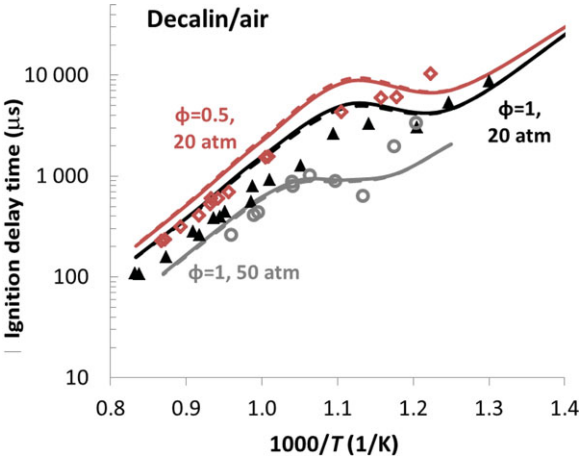

Figure 14 Decalin/air mixture over 1200–770 K at three conditions: $\Phi = 0.5$, 20 atm; $\Phi = 1.0$, 20 atm; $\Phi = 1.0$, 50 atm. Comparison of measured (symbols) [112] and predicted ignition delay times using the original (solid lines) and skeletal mechanism POLIMI_KEROSENE_231 (dashed lines). NTC behavior is evident at around 940–800 K.

geometry. Figure 15a shows a satisfactory comparison of experimental data and predictions of the original and skeletal model. Furthermore, the experimental data of the laminar flame speed of Jet A, as measured by Kumar et al. [114], are also reported in the same figure to highlight its similarity to this ternary surrogate. Moreover, using the binary Aachen surrogate (*n*-decane/TMB 80/20 wt) [24], Fig. 15b presents a

comparison between the laminar flame speeds of Jet A [114] and POSF 4658 (*n*-dodecane/isooctane/TMB/*n*-propyl benzene = 40.4/29.5/7.3/22.8 mol) [26] with the predictions of the original and lumped model, at 400 and 470 K. The experimental laminar flame speeds of a Jet A1 with a H/C of 1.98 are also reported [115], at 470 K. The laminar flame speeds are slightly higher than the previous ones at 400 K and lower at 470 K, thus indicating the ability also of Aachen surrogate to represent jet fuels.

Figures 16 and 17 show a couple of comparisons of experimental data of POSF 4658 surrogate oxidation with the predictions of the original and the reduced models [26]. The first set of experimental data refers to the variable pressure flow reactor at Princeton University, which was specifically employed to compare surrogate and real fuel reactivity over the low, negative temperature coefficient, and hot ignition regimes. The reactivity of this second generation surrogate is very similar to that of the ternary "first generation surrogate" (*n*-dodecane/isooctane/toluene of 42.7/33.0/24.3 mol%) [25], as shown in Fig. 15. The figure also indicates that model predictions closely reproduce these measurements. The second set of data refers to shock tube ignition delay experiments performed in the Rensselaer Polytechnic Institute facility [116]. The surrogate mixture already proved able to emulate the ignition delay of the target real fuel very closely at ~20 atm and air stoichiometric mixtures. Figure 17 again shows very similar predictions of the

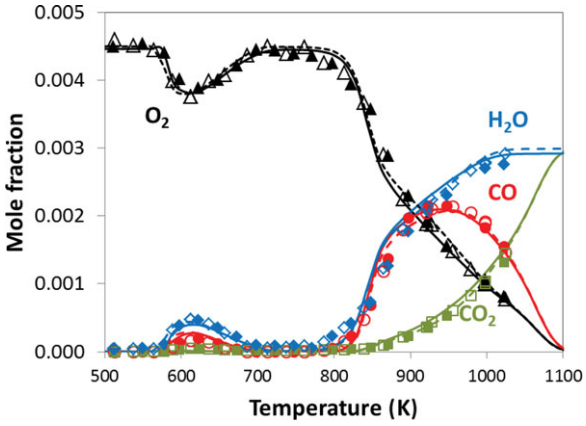

Figure 16 Oxidation of the first (empty symbols and dashed lines) and second (filled symbols and solid lines) generation of POSF 4658 surrogates in the Princeton variable pressure flow reactor. Experimental (symbols) and predictions of the original model (lines) [25,26].

complete kinetic scheme POLIMI_1404. They properly capture the NTC zone between 800 and 1000 K. The kinetic model slightly overestimates the ignition delay times, at low and high temperatures, while lower times are predicted in the NTC region. Moreover, the predictions of POLIMI_KEROSENE_HT_121 in the same figure indicates that the high-temperature mechanism is able to correctly predict the ignition delay times only at temperatures higher than 1100 K at 20 atm.

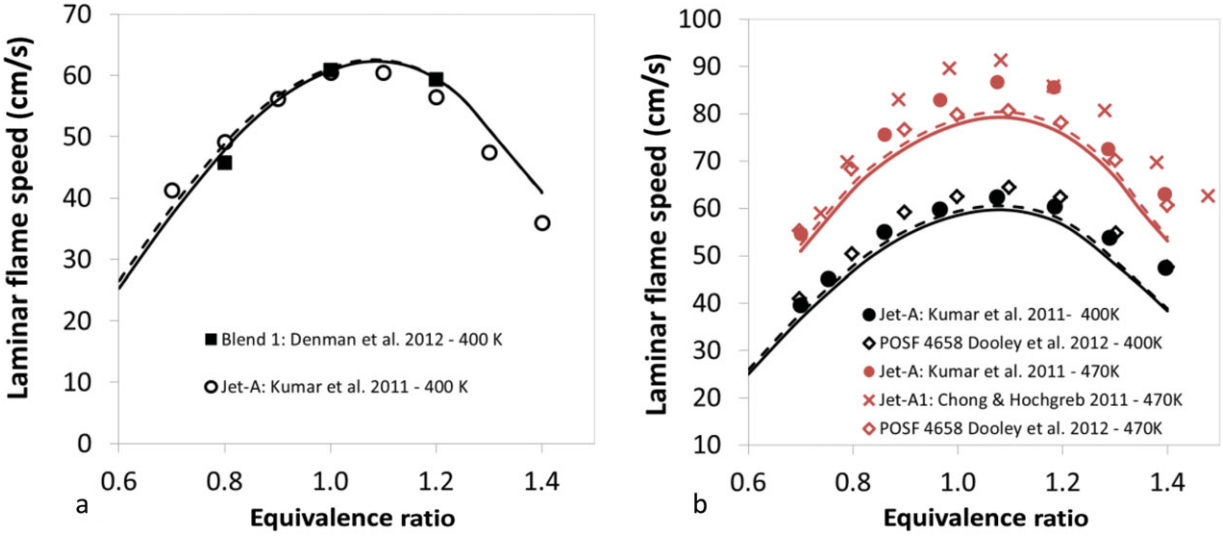

Figure 15 Laminar flame speed of Jet A and Jet A1. Panel a: Predicted and measured flame speed of Jet A and surrogate kerosene blend (*n*-decane (82%), methylcyclohexane (8%), toluene (10%)) at $T_{in} = 400$ K [113,114]. Panel b: Measured laminar flame speed of Jet A, Jet A1, and POSF 4658 [26,114,115] and predictions using the Aachen surrogate. Experimental (symbols) and predictions of the original (solid lines) and skeletal model POLIMI_KEROSENE_HT_121 (dashed lines).

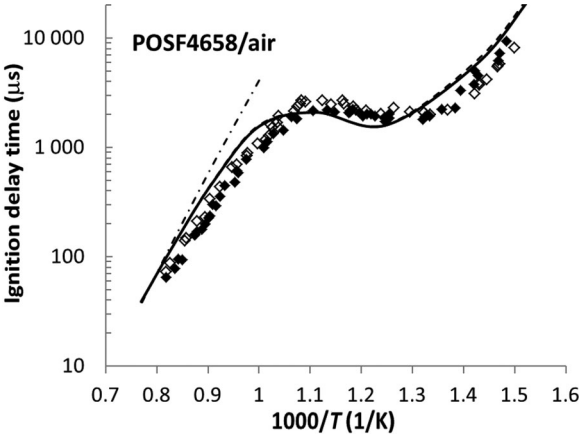

Figure 17 Shock tube ignition delay times of POSF 4658 oxidation with stoichiometric air at 20 atm. Experimental (symbols) [12] and predictions of the original (solid lines), the skeletal POLIMI_KEROSENE_231 (dashed lines), and the skeletal model POLIMI_KEROSENE_HT_121 (dotted–dashed lines).

A final application example of the reduced kinetic scheme POLIMI_KEROSENE_231 refers to a fuel derived from algal oils. As already mentioned, Gowdagiri et al. [41] analyzed the different ignition delay times of a conventional petroleum-derived military diesel fuel (F-76) and an alternative renewable fuel derived from hydroprocessing algal oils (HRD-76). Measurements were made in the reflected shock region for temperatures ranging from 671 to 1266 K, at 10 and 20 atm, and for fuel–air equivalence ratios of 0.5 and 1.0. The H/C of the HRD fuel is about 2.12, showing a quasi-complete hydrogenation of the fuel, whereas the ratio of the original fuel was only 1.8. Panel a of Fig. 18 shows a comparison of measured and predicted ignition delay times of the military diesel fuel F-76 at 20 atm and fuel–air equivalence ratios of 0.5 and 1.0. According to fuel specifications, a five-component surrogate mixture (*n*-hexadecane/isocetane/methylcyclohexane/propyl-benzene/dialin = 53/18/8/15/6 mol) was assumed. Panel b of the same figure compares the ignition delay times of the original and the hydrotreated fuels, at 20 atm and fuel–air equivalence ratios of 0.5. The model predictions agree with the measurements and show that at high temperatures the reactivity of the two fuels is indistinguishable, whereas at low temperatures the ignition delay time for HRD-76 is up to a factor of two shorter than F-76, due to the larger fraction of *n*-paraffins and lack of aromatics. HRD-76 is characterized by a similar amount of linear and branched alkanes. The reference species isocetane is 2,2,4,4,6,8,8 heptamethyl-nonane, whereas a more limited methylation degree is present in branched alkanes from hydrotreating processes. As already discussed by Won et al. [117] in analyzing surrogate mixtures for 2,6,10 trimethyl dodecane, the methylene (CH_2) to methyl (CH_3) ratio globally correlates the low-temperature alkylperoxy radical reactivity, for large branched alkanes. Thus, a surrogate mixture containing only 20% of isocetane is considered in the comparisons of Panel b. Both panels of Fig. 18 again confirm that the predictions of the original and the reduced scheme are very similar.

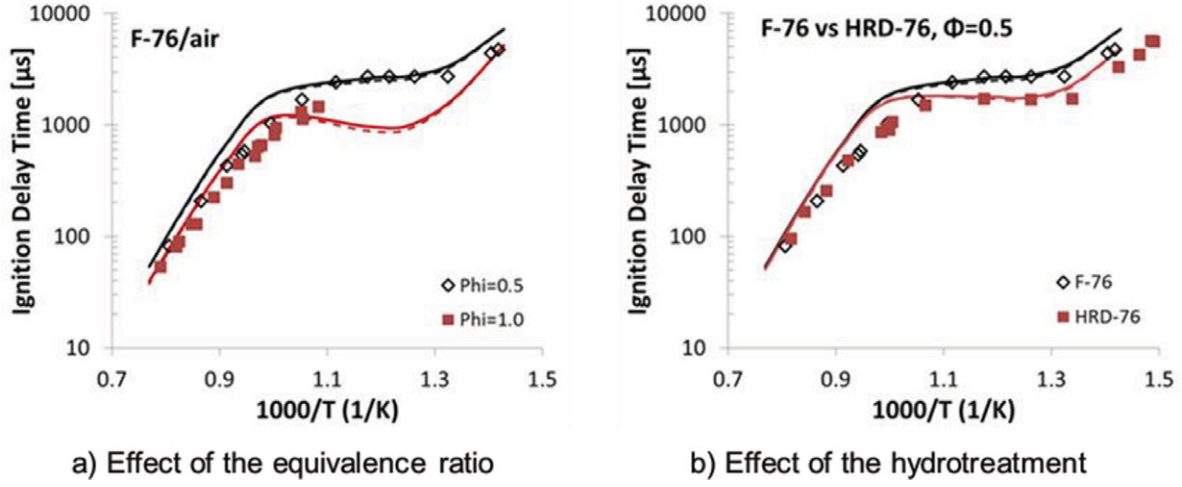

Figure 18 Shock tube ignition delay times of the fuel F-76 and the hydrotreated HRD-76, at 20 atm and different fuel–air equivalence ratios. Experimental (symbols) [41] and predictions of the original (solid lines), and the skeletal POLIMI_KEROSENE_231 (dashed lines).

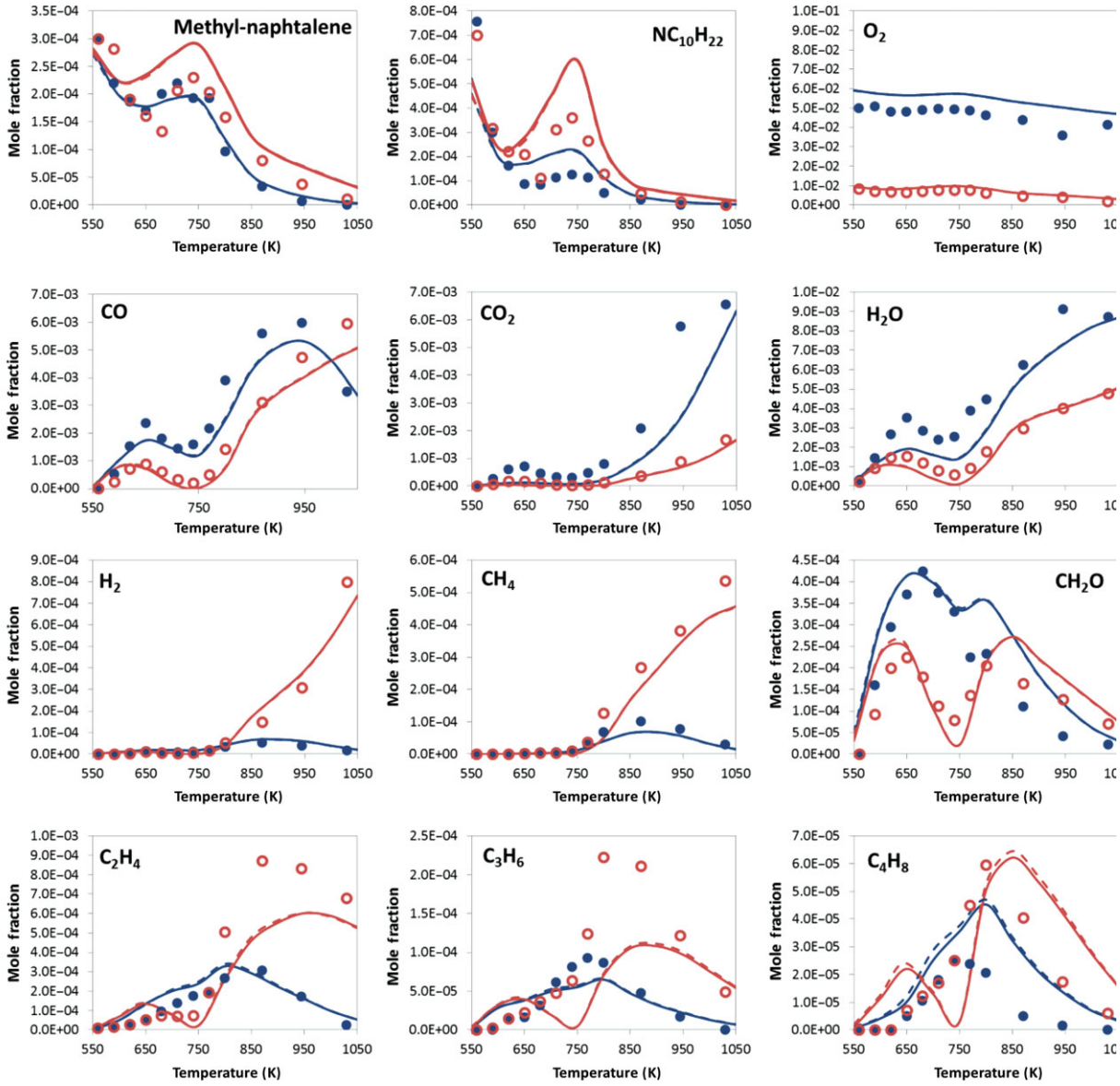

Figure 19 Oxidation of a *n*-decane/methyl–naphthalene mixture (70/30 in mol) in a jet-stirred reactor at 10 atm and 1.0 s [122]. Mole fractions of fuels and major species. Experimental data at $\Phi = 0.25$ (filled circles) and $\Phi = 1.5$ (empty circles). Predictions: original (continuous lines) and reduced model POLIMI_DIESEL_201 (dashed lines).

Skeletal Kinetic Schemes of Diesel Fuel

Skeletal Kinetic Scheme of Diesel Fuel (n-Alkanes, Isoalkanes, Toluene, Xylene, and Methyl-naphthalene). The skeletal mechanism *POLIMI_DIESEL_201* refers to *n*-alkanes up to *n*-hexadecane, toluene, xylene, and methyl-naphthalene. Surrogate mixtures including *n*-decane as reference species of *n*-alkanes and α-methylnaphthalene to represent polyaromatic compounds were extensively used by several authors to represent diesel fuels [118–121]. More recently, the oxidation of this binary diesel surrogate mixture (70% *n*-decane/30% α-methylnaphthalene in moles) was performed by Ramirez et al. [122] in a jet-stirred reactor at 560–1030 K, 10 atm, with 10,300 ppm of carbon and equivalence ratios of 0.25–1.5. Figure 19 shows a detailed and adequate comparison of experimental data and the predictions of original and reduced kinetic schemes.

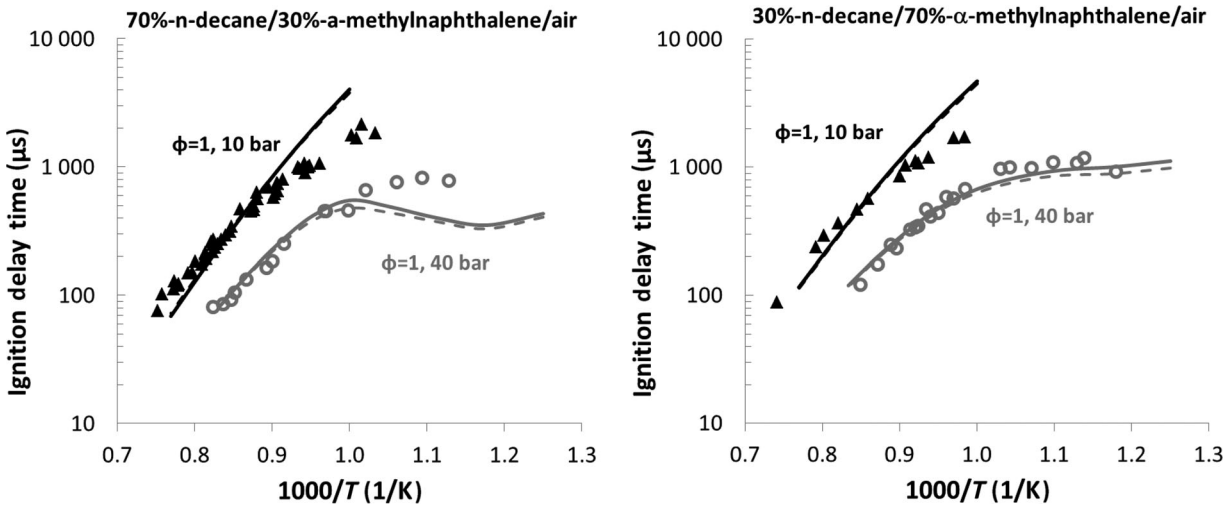

Figure 20 Ignition delay times of *n*-decane/α-methylnaphthalene mixtures in air. Left panel: 70/30 (mol). Right panel: 30/70 (mol). Comparison between experimental data [123] and model predictions. Complete mechanism: continuous lines. Reduced mechanism POLIMI_DIESEL_201: dotted lines.

Further experimental data in a shock tube device were discussed by Wang et al. [123]. Figure 20 shows a comparison of model predictions with the experimental data of ignition delay times of stoichiometric mixtures of *n*-decane/α-methyl-naphthalene in air, at high pressures. Model predictions are in good agreement with the experimental data for the entire pressure and temperature ranges especially for the 30 *n*-decane/70 α-methylnaphthalene blend. The figure also shows that the NTC behavior is overestimated at 40 bar for the 70/30 mixture. A very similar discrepancy was also observed by Wang et al. [123], who predicted the ignition delay times using a mechanism with nearly 700 species and 4000 reactions. To better investigate this point, and since the reactivity of this mixture is dominated by the *n*-decane chemistry, Fig. 21 shows a comparison of model predictions with the ignition delay times of pure *n*-decane air stoichiometric mixtures at different pressures. It is interesting to note that the data of Pfahl et al. [124] agree with the similar measurements of Shen et al. [125] at 11–12 bar, whereas at 40–50 bar there is a significant discrepancy in the NTC region, very similar to the one observed in the 30 α-methylnaphthalene /70 n-decane blend of Fig. 20.

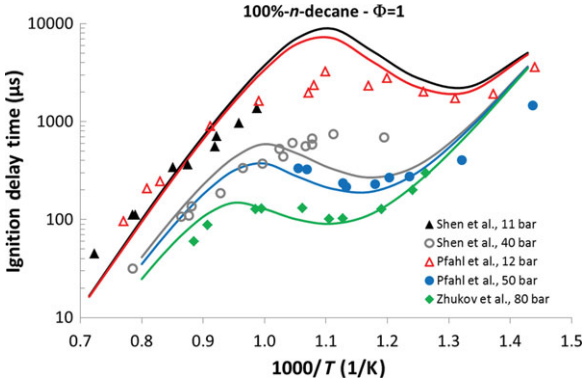

Figure 21 Ignition delay times of *n*-decane in air at different pressures. Comparison between experimental data [124,125,161] and complete model predictions (lines).

Skeletal Kinetic Scheme of Biodiesel Fuels (Heavy Methyl Esters). As already discussed in Saggese et al. [80], a lumped approach to the oxidation of heavy methyl esters simply required the extension of the overall kinetic mechanism with about 60 new lumped species, with a relevant saving in respect of the more than 3000 species involved in the detailed kinetics [39,126]. Furthermore, Stagni et al. [127] already derived from the overall lumped scheme POLIMI the reduced mechanism of oxidation of methyl esters POLIMI_FAME_177. According to the composition of common biodiesel fuels in terms of fatty acids [128], the inlet composition to derive the skeletal model was taken as the molar average of soybean, rapeseed and palm oil, always referring to the operating conditions of Table VII.

Ignition delay times for different low-vapor-pressure biodiesel surrogates were recently measured behind reflected shock waves, using an aerosol shock tube at Stanford by Campbell et al. [129]. These fuels included methyl decanoate, methyl laurate

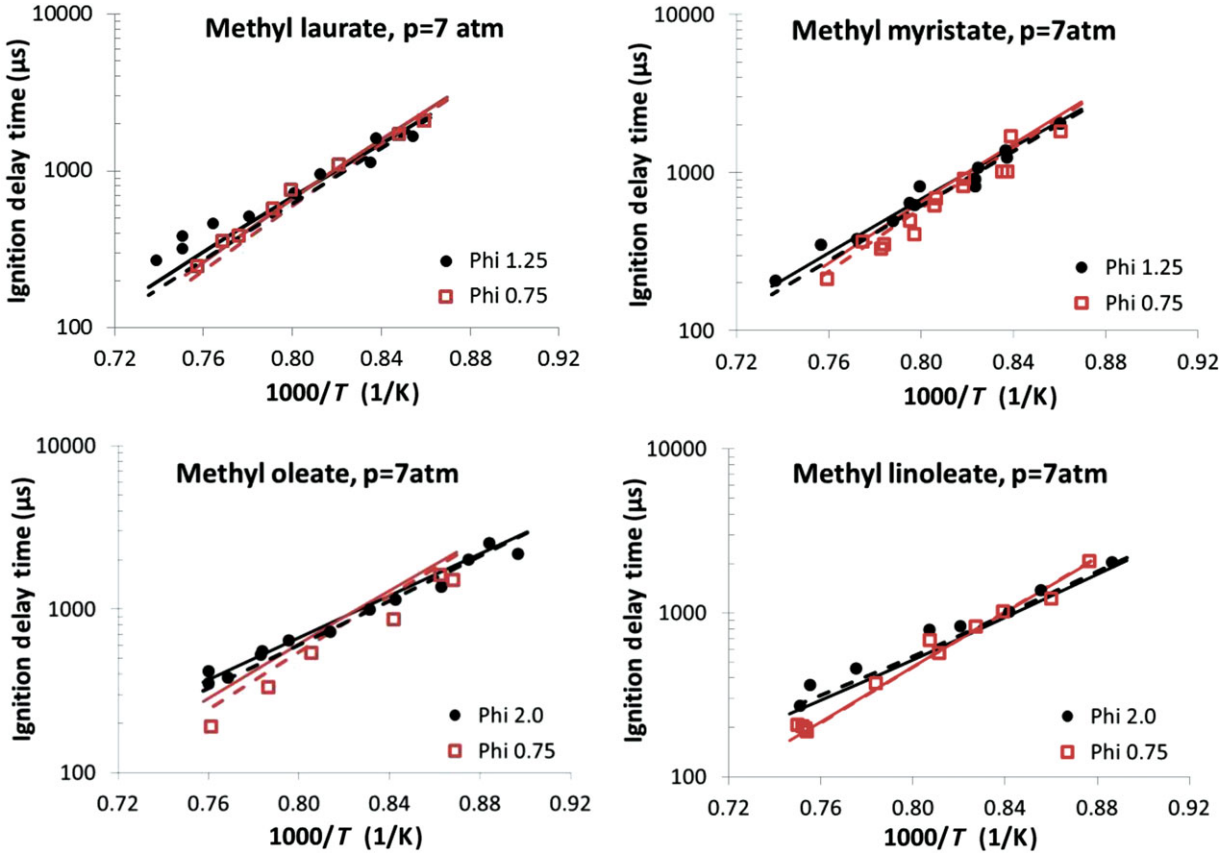

Figure 22 Methyl ester ignition delay times in 4% oxygen/argon mixtures, at 7 atm, and different equivalence ratios [129,131]. Experiments (symbols) are compared with the original (solid lines) and the reduced kinetic model POLIMI_FAME_177 (dashed lines).

($C_{13}H_{26}O_2$), methyl myristate ($C_{15}H_{30}O_2$), and methyl palmitate ($C_{17}H_{34}O_2$), all of which have a fully saturated alkane chemical structure. A blend of methyl oleate ($C_{19}H_{36}O_2$) with 30% FAME was also examined. Experiments were conducted in 4% oxygen/argon mixtures, at temperatures from 1026 to 1388 K, pressure of 7.0 atm, and equivalence ratios 0.75 and 1.25. The oxidation of methyl decanoate ($C_{11}H_{22}O_2$) was also studied and well compared with previous experimental data [130]. Figure 22 shows a comparison of the experimental ignition delay times with the predictions of the original and the reduced kinetic model for different methyl esters. On the basis of a vertical lumping approach, only methyl decanoate (MD) and methyl palmitate (MPA) are assumed as reference species of saturated methyl esters. Intermediate species are derived with the lever rule; thus the following MD/MPA mixtures identically represent methyl laurate (MLA = 2/1) and methyl myristate (MMY = 1/2). The reliability of the vertical lumping is supported by the fact that the structures of MD, MLA, MMY, and MPA are identical except that the carbon chain length moves from 10 for MD up to 16 for MPA. A comparison among these sets of data reveals that ignition delay time slightly and progressively decreases as the carbon chain length increases from MLA to MPA. Figure 22 first confirms the reliability of the lumped model of methyl esters [80], also in comparison with the new experimental data of MLA and MMY, as well as with the data of methyl oleate and methyl linoleate of Campbell et al. [131], then shows that the reduced model fully agree with the original one.

Similar good agreements are also observed in Fig. 23 between the model predictions and the comparison with the experimental data of the oxidation of rapeseed methyl ester in the Orléans JSR, at temperatures from 800 to 1400 K, different equivalence ratios, and pressures of 1 and 10 atm [132]. All the experiments used highly diluted RME (0.05% fuel)/O_2/N_2 mixtures. Model predictions are obtained by assuming the following RME composition: 44.2 palmitate, 4.5 stearate, 40.8 oleate, 10.2 linoleate and 0.2 methyl linolenate.

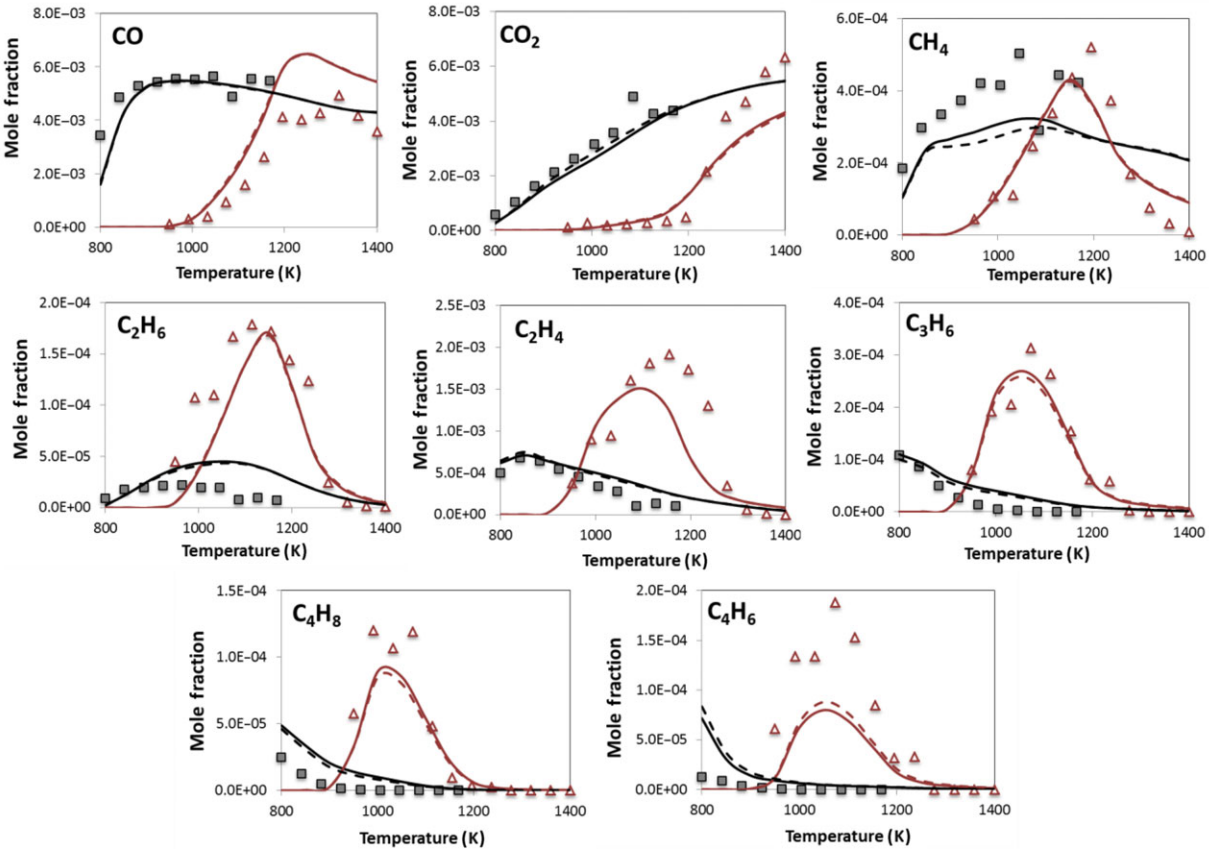

Figure 23 Pressure effect on the stoichiometric oxidation of rapeseed methyl ester [132]. Comparisons of experimental data (1 atm and 0.07 s: squares; 10 atm and 1 s: triangles) and original (solid lines) and skeletal model predictions POLIMI_FAME_177 (dashed lines).

Skeletal Kinetic Scheme of Diesel/Biodiesel Fuels. The skeletal mechanism of diesel and biodiesel fuel POLIMI_DIESEL_FAME_226 refers to heavy *n*-alkanes, aromatics, methyl-naphthalene, and heavy methyl esters. Figure 24 shows a sample of comparison among experimental data and predictions of detailed and reduced models. These data refer to the atmospheric and stoichiometric air oxidation of *n*-decane mixtures with methyl-palmitate [133] and with methyl-oleate [134]. Both reduced and original models agree with experimental data, being the deviations between the two models well within the experimental uncertainties.

A final comparison between experimental data and model predictions refers to the oxidation of a B30 biodiesel surrogate fuel (49% *n*-decane, 21% α-methylnaphthalene, and 30% methyl-octanoate in moles) [43]. This surrogate was satisfactorily used to mimic the combustion behavior of a commercial B30 (30% FAME by vol.) biodiesel fuel. Experiments were performed in a jet-stirred reactor at 560–1030 K, 6 and 10 atm, with equivalence ratios of 0.25–1.5, and 10,300 ppm of carbon. Figure 25 shows a comparison of reduced and original models with the experimental data at equivalence ratios 0.5 and 1.5. Both models fairly agree also in respect of minor species, largest deviations are observed for the few ppm of benzene. The overall agreement with these experimental measurements is reasonable and comparable with the one reported by Ramirez et al. [43], by using a detailed and tailored kinetic scheme involving 1964 species and 7748 reactions.

CORE KINETIC MECHANISM C_0-C_4

Figure 26 schematically depicts the involved species in the different skeletal oxidation mechanisms, and it also highlights that, due to the hierarchical modularity of the kinetic schemes, several species belongs to the

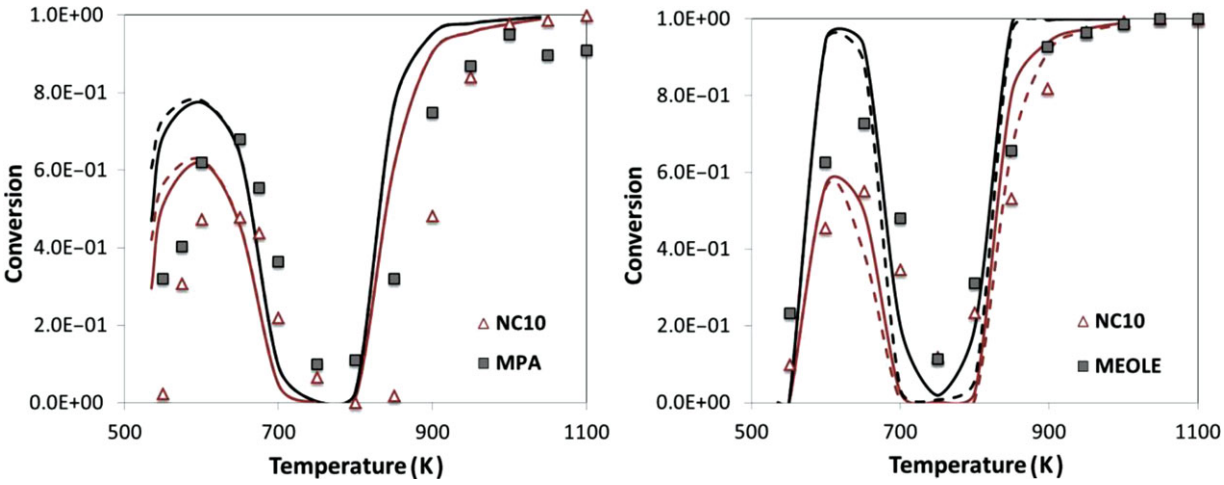

Figure 24 Conversion of atmospheric and stoichiometric air oxidation of *n*-decane mixtures at 1.5 s: Panel (a) with 26% methyl palmitate [133], Panel (b) with 26% methyl oleate [134]. Comparisons of experimental (symbols) and predicted conversion with the original (solid lines) and skeletal model POLIMI_DIESEL_FAME_226 (dashed lines).

same core kinetic mechanism C_0–C_4. All the mechanisms involve several fuel specific species required to characterize the primary propagation reactions. Moreover, while the characterization of the low-temperature ignition in internal combustion engines could require a large detail of peroxide species, the kinetic modeling of high temperature sooting flames unavoidably involves several aromatic and PAH up to very high molecular weights.

Thus, all the reduced skeletal mechanisms contain almost the same core chemistry involving C_0–C_4 species. The sensitivity coefficients of laminar flame speed on reaction rate coefficients for heavy fuels clearly highlight that the most sensitive reactions belong to the C_0–C_4 submechanism [85]. This fact is further confirmed by the recent work of Li et al. [109] on the laminar flame of isocetane/air and decalin/air mixtures. Results revealed that the oxidation of both fuels in flames is largely sensitive to H_2/CO and C_1–C_4 small hydrocarbon chemistry, whereas fuel-specific reactions play a minor role on flame propagation [109]. In fact, fuel-specific reactions occur upstream of the main reaction zone, and thus reactions including heavier species do not have significant effect on the high-temperature combustion.

Therefore, the core mechanism is very important not only for modeling combustion features of natural gas and gaseous fuels but also for the correct characterization of the oxidation process of all the liquid transportation fuels and related surrogate mixtures. In fact, the reactivity of these small fuels and intermediates is of critical importance in understanding the combustion characteristics, such as ignition delay times, flame speeds, and emissions of practical fuels (NO*x*, PAHs, soot). GRI-Mech [135], among the first kinetic scheme freely available on the Internet to the combustion community, is an optimized mechanism specifically designed to simulate natural gas combustion, including NO*x* formation. Several kinetic mechanisms are freely available (see, for instance, San Diego Mech [136], USC Mech [137], LLNL [39], NUIG [138], Nancy [57], and POLIMI mechanism [85]). All these mechanisms are similar in the structure, involve similar reactions often with different rate constants; they are not validated in the same conditions and perform differently depending on the fuels and combustion conditions. Following the pioneering work of GRI Mech [139] and PRIME [140], and aiming at an useful identification of an optimal core mechanism, recent kinetic efforts are and still need to be significantly addressed to improve the accuracy of detailed reaction mechanism in the C_0–C_2 [138] and the C_0–C_4 range [141], over a broad range of conditions.

CONCLUSIONS

The lumped POLIMI pyrolysis and oxidation mechanism of hydrocarbon and oxygenated fuels has been used for generating several skeletal mechanisms for typical surrogate mixtures, moving from pure *n*-heptane up to heavy diesel fuels. All these skeletal models are simply reduced with a RFA, and they involve between 100 and 200 species. As already discussed in a previous paper [127], the skeletal models are not very sensitive to the adopted reduction

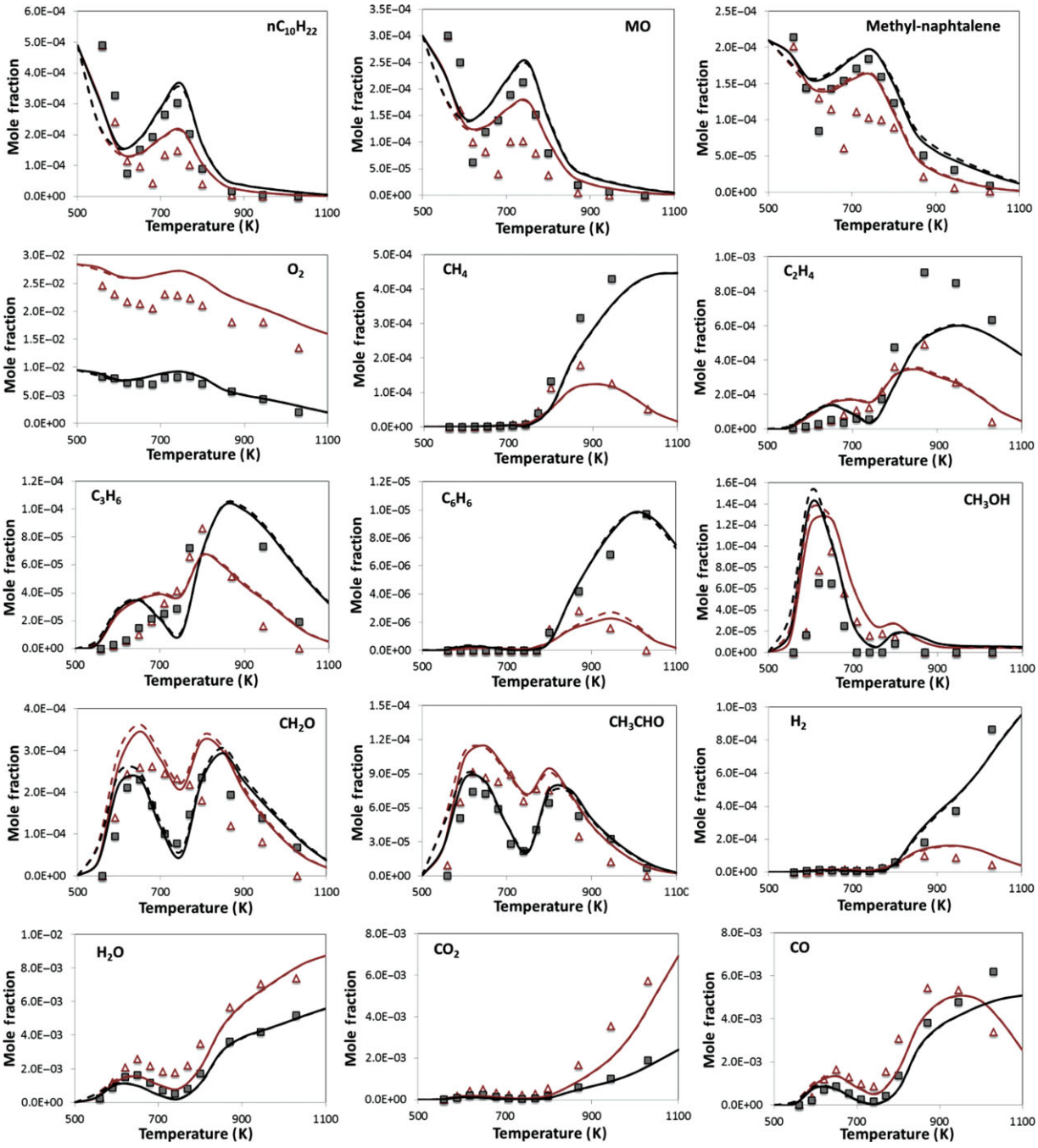

Figure 25 Oxidation of a *n*-decane/methyl-naphthalene/methyl-octanoate mixture (49/21/30 in mol) in a jet-stirred reactor at 10 atm and 1 s [43]. Mole fractions of fuels and major species experimental data at $\Phi = 0.5$ (triangles) and $\Phi = 1.5$ (squares). Predictions: original (continuous lines) and reduced model POLIMI_DIESEL_FAME_226 (dashed lines).

methods, but mainly depend on the characteristics and dimensions of the original mechanism. Thus, with the same accuracy, the skeletal models of gasoline primary reference fuels obtained from the lumped POLIMI model contain about one third of the species in respect of the similar skeletal models obtained from detailed mechanisms [47]. Similar conclusions were also derived for the reduced model of *n*-dodecane oxidation [63]. The number of species of these reduced models already allows detailed CFD calculations in internal combustion engines [87], and these skeletal kinetic mechanisms maintain the standard structure of

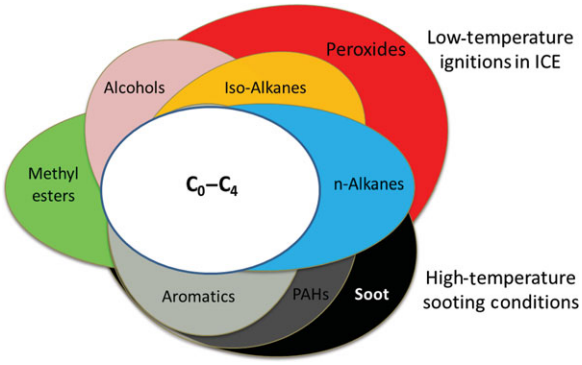

Figure 26 Species involved in the different skeletal oxidation mechanisms.

the kinetic scheme, without modifications of the reactions contained in the original mechanism. Of course, successive reduction phases, usually tailored to specific and optimized solvers, are necessary when the interest is toward more complex CFD computations [86].

Owing to the interest toward a greater use of renewable fuels, skeletal models of biogasolines containing light alcohols, as well as skeletal models of biodiesel fuels, including fatty acid methyl esters are also presented and discussed. The whole set of comparisons with experimental data obtained in a wide range of conditions further contribute to validate not only of the different reduced model but also the complete model POLIMI_1404.

Authors gratefully acknowledge Dr. Philippe Dagaut for providing the data of Figs 19, 23, and 25.

BIBLIOGRAPHY

1. Pitz, W. J.; Mueller, C. J. Prog Energy Combust Sci 2011, 37, 330–350.
2. Bunting, B. G. Final Report for NFE-07–00912, Oak Ridge National Laboratory, Oak Ridge, TN, 2012.
3. McIlroy, A.; McRae, G.; Sick, V.; Siebers, D. L.; Westbrook, C. K.; Smith, P. J.; Taatjes, C.; Trouve, A.; Wagner, A. F.; Rohlfing, E.; Manley, D.; Tully, F.; Hilderbrandt, R.; Marceau, D.; Oneal, J.; Lyday, M.; Cebulski, F.; Garcia, T. R.; Strong, D., Basic Research Needs for Clean and Efficient Combustion of 21st Century Transportation Fuels. 2006. http://science.energy.gov/~/media/bes/pdf/reports/files/ctf_rpt.pdf (access date January 2014).
4. Janssen, A. J.; Kremer, F. W.; Baron, J. H.; Muether, M.; Pischinger, S.; Klankermayer, J. Energy Fuels 2011, 25, 4734–4744.
5. Concawe. 2013. https://www.concawe.eu/ (accessed 31 January 2014).
6. Lonza, L.; Hass, H.; Maas, H.; Reid, A.; Rose, K. D. JRC, EUCAR and CONCAWE 2011, 70.
7. Niemeyer, K. E.; Sung, C.-J.; Raju, M. P. Combust Flame 2010, 157, 1760–1770.
8. Edwards, T.; Maurice, L. Q. J Propul Power 2001, 17, 461–466.
9. Violi, A.; Yan, S.; Eddings, E. G.; Sarofim, A. F.; Granata, S.; Faravelli, T.; Ranzi, E. Combust Sci Technol 2002, 174, 399–417.
10. Peralta-Yahya, P. P.; Zhang, F.; Del Cardayre, S. B.; Keasling, J. D. Nature 2012, 488, 320–328.
11. Mehl, M.; Faravelli, T.; Giavazzi, F.; Ranzi, E.; Scorletti, P.; Tardani, A.; Terna, D. Energy & Fuels 2006, 20, 2391–2398.
12. Gauthier, B. M.; Davidson, D. F.; Hanson, R. K. Combust Flame 2004, 139, 300–311.
13. Davidson, D.; Gauthier, B.; Hanson, R. Proc Combust Inst 2005, 30, 1175–1182.
14. Naik, C. V.; Pitz, W. J.; Sjöberg, M.; Dec, J. E.; Orme, J.; Curran, H. J.; Simmie, J. M.; Westbrook, C. K. SAE paper 3741, 2005.
15. Mehl, M.; Pitz, W. J.; Westbrook, C. K.; Curran, H. J. Proc Combust Inst 2011, 33, 193–200.
16. Lindstedt, R. P.; Maurice, L. Q. Combust Sci Technol 1995, 107, 317–353.
17. Hudgens, J. W. (Ed.); Workshop on Combustion Simulation Databases for Real Transportation Fuels, NIST, Gaithersburg, MD, 2003.
18. Agosta, A.; Cernansky, N. P.; Miller, D. L.; Faravelli, T.; Ranzi, E. Exp Ther Fluid Sci 2004, 28, 701–708.
19. Humer, S.; Frassoldati, A.; Granata, S.; Faravelli, T.; Ranzi, E.; Seiser, R.; Seshadri, K. Proc Combust Inst 2007, 31, 393–400.
20. Saffaripour, M.; Kholghy, M.; Dworkin, S.; Thomson, M. Proc Combust Inst 2013, 34, 1057–1065.
21. Eddings, E. G.; Yan, S.; Ciro, W.; Sarofim, A. F. Combust Sci Technol 2005, 177, 715–739.
22. Montgomery, C. J.; Cannon, S. M.; Mawid, M. A.; Sekar, B. DTIC Document, 2002.
23. Riesmeier, E.; Honnet, S.; Peters, N. J Eng Gas Turbines Power 2004, 126, 899–905.
24. Honnet, S.; Seshadri, K.; Niemann, U.; Peters, N. Proc Combust Inst 2009, 32, 485–492.
25. Dooley, S.; Won, S. H.; Chaos, M.; Heyne, J.; Ju, Y.; Dryer, F. L.; Kumar, K.; Sung, C.-J.; Wang, H.; Oehlschlaeger, M. A. Combust Flame 2010, 157, 2333–2339.
26. Dooley, S.; Won, S. H.; Heyne, J.; Farouk, T. I.; Ju, Y.; Dryer, F. L.; Kumar, K.; Hui, X.; Sung, C.-J.; Wang, H. Combust Flame 2012, 159, 1444–1466.
27. Widegren, J. A.; Bruno, T. J. Ind Eng Chem Res 2008, 47, 4342–4348.
28. Xiao, G.; Zhang, Y.; Lang, J. Ind Eng Chem Res 2013, 52, 3732–3741.
29. Lin, R.; Tavlarides, L. L. J Supercrit Fluids 2012, 71, 136–146.
30. Hasegawa, R.; Sakata, I.; Koyama, T.; Yanagihara, H. Training 2003, 2014, 02–24.

31. Noel, L.; Maroteaux, F.; Ahmed, A. Combustion 2004, 1, 1914.
32. Mueller, C. J.; Cannella, W. J.; Bruno, T. J.; Bunting, B.; Dettman, H. D.; Franz, J. A.; Huber, M. L.; Natarajan, M.; Pitz, W. J.; Ratcliff, M. A. Energy Fuels 2012, 26, 3284–3303.
33. Krishnasamy, A.; Ra, Y.; Reitz, R. D.; Bunting, B. Energy Fuels 2011, 25, 1474–1484.
34. Huber, G. W.; Iborra, S.; Corma, A. Chem Rev 2006, 106, 4044–4098.
35. Demirbas, A. Appl Energy 2011, 88, 17–28.
36. Román-Leshkov, Y.; Barrett, C. J.; Liu, Z. Y.; Dumesic, J. A. Nature 2007, 447, 982–985.
37. Van Geem, K. M.; Cuoci, A.; Frassoldati, A.; Pyl, S. P.; Marin, G. B.; Ranzi, E. Combust Sci Technol 2012, 184, 942–955.
38. Semelsberger, T. A.; Borup, R. L.; Greene, H. L. J Power Sources 2006, 156, 497–511.
39. Westbrook, C. K.; Naik, C. V.; Herbinet, O.; Pitz, W. J.; Mehl, M.; Sarathy, S. M.; Curran, H. J. Combust Flame 2011, 158, 742–755.
40. Luning Prak, D. J.; Cowart, J. S.; Hamilton, L. J.; Hoang, D. T.; Brown, E. K.; Trulove, P. C. Energy Fuels 2013, 27, 954–961.
41. Gowdagiri, S.; Wang, W.; Oehlschlaeger, M. A. Fuel 2014, 128, 21–29.
42. Westbrook, C. K.; Pitz, W. J.; Herbinet, O.; Curran, H. J.; Silke, E. J. Combust Flame 2009, 156, 181–199.
43. Ramirez, H. P.; Hadj-Ali, K.; Diévart, P.; Dayma, G.; Togbé, C.; Moréac, G.; Dagaut, P. Proc Combust Inst 2011, 33, 375–382.
44. Wang, H.; Dames, E.; Sirjean, B.; Sheen, D. A.; Tangko, R.; Violi, A.; Lai, J. Y. W.; Egolfopoulos, F. N.; Davidson, D. F.; Hanson, R. K. JetSurF version 2010, 2, 19.
45. Lu, T. F.; Law, C. K. Prog Energy Combust Sci 2009, 35, 192–215.
46. McIlroy, A.; McRae, G.; Sick, V.; Siebers, D.; Westbrook, C.; Smith, P.; Taatjes, C.; Trouve, A.; Wagner, A.; Rohlfing, E. DOESC (USDOE Office of Science (SC)), 2006.
47. Saylam, A.; Ribaucour, M.; Pitz, W. J.; Minetti, R. International Journal of Chemical Kinetics 2007, 39, 181–196.
48. Ra, Y.; Reitz, R. D. Combust Flame 2008, 155, 713–738.
49. Westbrook, C. K.; Warnatz, J.; Pitz, W. J. In Symposium (International) on Combustion, 1989, pp 893–901.
50. Ranzi, E.; Faravelli, T.; Gaffuri, P.; Sogaro, A. Combust Flame 1995, 102, 179–192.
51. Curran, H. J.; Gaffuri, P.; Pitz, W. J.; Westbrook, C. K. Combust Flame 1998, 114, 149–177.
52. Buda, F.; Bounaceur, R.; Warth, V.; Glaude, P.-A.; Fournet, R.; Battin-Leclerc, F. Combust Flame 2005, 142, 170–186.
53. Ranzi, E.; Faravelli, T.; Gaffuri, P.; Garavaglia, E.; Goldaniga, A. Ind Eng Chem Res 1997, 36, 3336–3344.
54. Ranzi, E.; Frassoldati, A.; Granata, S.; Faravelli, T. Ind Eng Chem Res 2005, 44, 5170–5183.
55. Herbinet, O.; Husson, B.; Serinyel, Z.; Cord, M.; Warth, V.; Fournet, R.; Glaude, P.-A.; Sirjean, B.; Battin-Leclerc, F.; Wang, Z. Combust Flame 2012, 159, 3455–3471.
56. Fournet, R.; Battin-Leclerc, F.; Glaude, P. A.; Judenherc, B.; Warth, V.; Come, G. M.; Scacchi, G.; Ristori, A.; Pengloan, G.; Dagaut, P. Int J Chem Kinet 2001, 33, 574–586.
57. Battin-Leclerc, F. Prog Energy Combust Sci 2008, 34, 440–498.
58. Glaude, P. A.; Herbinet, O.; Bax, S.; Biet, J.; Warth, V.; Battin-Leclerc, F. Combust Flame 2010, 157, 2035–2050.
59. Ranzi, E.; Dente, M.; Goldaniga, A.; Bozzano, G.; Faravelli, T. Prog Energy Combust Sci 2001, 27, 99–139.
60. Wang, H.; Frenklach, M. Combust Flame 1991, 87, 365–370.
61. Lu, T. F.; Law, C. K. Proc Combust Inst 2005, 30, 1333–1341.
62. Stagni, A.; Cuoci, A.; Frassoldati, A.; Faravelli, T.; Ranzi, E. Ind Eng Chem Res 2014, 53(22), 9004-9016
63. Narayanaswamy, K.; Pepiot, P.; Pitsch, H. Combust Flame 2013.
64. Ranzi, E.; Dente, M.; Pierucci, S.; Biardi, G. Ind Eng Chem Fundam 1983, 22, 132–139.
65. Ranzi, E.; Sogaro, A.; Gaffuri, P.; Pennati, G.; Westbrook, C. K.; Pitz, W. J. Combust Flame 1994, 99, 201–211.
66. Ranzi, E.; Gaffuri, P.; Faravelli, T.; Dagaut, P. Combust Flame 1995, 103, 91–106.
67. Ranzi, E.; Faravelli, T.; Gaffuri, P.; Sogaro, A.; D'Anna, A.; Ciajolo, A. Combust Flame 1997, 108, 24–42.
68. Granata, S.; Faravelli, T.; Ranzi, E. Combust Flame 2003, 132, 533–544.
69. Cavallotti, C.; Rota, R.; Faravelli, T.; Ranzi, E. Proc Combust Inst 2007, 31, 201–209.
70. Cooke, J. A.; Bellucci, M.; Smooke, M. D.; Gomez, A.; Violi, A.; Faravelli, T.; Ranzi, E. Proc Combust Inst 2005, 30, 439–446.
71. Mehl, M.; Vanhove, G.; Pitz, W. J.; Ranzi, E. Combust Flame 2008, 155, 756–772.
72. Ranzi, E. Energy Fuels 2006, 20, 1024–1032.
73. Ranzi, E. In Combustion Generated Fine Carbonaceous Particles: Proceedings of an International Workshop, Villa Orlandi, Anacapri, Italy, May 13–16, 2007.
74. Frassoldati, A.; Cuoci, A.; Faravelli, T.; Ranzi, E. Combust Sci Technol 2010, 182, 653–667.
75. Grana, R.; Frassoldati, A.; Faravelli, T.; Niemann, U.; Ranzi, E.; Seiser, R.; Cattolica, R.; Seshadri, K. Combust Flame 2010, 157, 2137–2154.

76. Frassoldati, A.; Grana, R.; Faravelli, T.; Ranzi, E.; Oßwald, P.; Kohse-Höinghaus, K. Combust Flame 2012, 159, 2295–2311.
77. Frassoldati, A.; Faravelli, T.; Ranzi, E.; Kohse-Höinghaus, K.; Westmoreland, P. R. Combust Flame 2011, 158, 1264–1276.
78. Grana, R.; Frassoldati, A.; Cuoci, A.; Faravelli, T.; Ranzi, E. Energy 2012, 43, 124–139.
79. Grana, R.; Frassoldati, A.; Saggese, C.; Faravelli, T.; Ranzi, E. Combust Flame 2012, 159, 2280–2294.
80. Saggese, C.; Frassoldati, A.; Cuoci, A.; Faravelli, T.; Ranzi, E. Proc Combust Inst 2013, 34, 427–434.
81. Oehlschlaeger, M. A.; Shen, H. P. S.; Frassoldati, A.; Pierucci, S.; Ranzi, E. Energy Fuels 2009, 23, 1464–1472.
82. Dagaut, P.; Ristori, A.; Frassoldati, A.; Faravelli, T.; Dayma, G.; Ranzi, E. Proc Combust Inst 2013, 34, 289–296.
83. Dagaut, P.; Ristori, A.; Frassoldati, A.; Faravelli, T.; Dayma, G.; Ranzi, E. Energy Fuels 2013, 27, 1576–1585.
84. Saggese, C.; Frassoldati, A.; Cuoci, A.; Faravelli, T.; Ranzi, E. Combust Flame 2013, 160, 1168–1190.
85. Ranzi, E.; Frassoldati, A.; Grana, R.; Cuoci, A.; Faravelli, T.; Kelley, A. P.; Law, C. K. Prog Energy Combust Sci 2012, 38, 468–501.
86. Lu, T.; Law, C. K. Combust Flame 2008, 154, 153–163.
87. D'Errico, G.; Lucchini, T.; Stagni, A.; Frassoldati, A.; Faravelli, T.; Ranzi, E. SAE Paper 24-0014, 2013.
88. Cuoci, A.; Frassoldati, A.; Faravelli, T.; Ranzi, E. In XXXIV Meeting of the Italian Section of the Combustion Institute, Rome, 2011.
89. Manenti, F.; Dones, I.; Buzzi-Ferraris, G.; Preisig, H. A. Ind Eng Chem Res 2009, 48, 9979–9984.
90. Buzzi-Ferraris, G.; Manenti, F. BzzMath: Comput-Aided Chem Eng 2012, 30, 1312–1316.
91. Dagaut, P.; Reuillon, M.; Cathonnet, M. Combust Flame 1995, 101, 132–140.
92. Sileghem, L.; Alekseev, V. A.; Vancoillie, J.; Van Geem, K. M.; Nilsson, E. J. K.; Verhelst, S.; Konnov, A. A. Fuel 2013, 112, 355–365.
93. Curran, H. J.; Gaffuri, P.; Pitz, W. J.; Westbrook, C. K. Combust Flame 2002, 129, 253–280.
94. Luong, M. B.; Luo, Z. Y.; Lu, T. F.; Chung, S. H.; Yoo, C. S. Combust Flame 2013, 160, 2038–2047.
95. Sileghem, L.; Alekseev, V. A.; Vancoillie, J.; Nilsson, E. J. K.; Verhelst, S.; Konnov, A. A. Fuel 2014, 115, 32–40.
96. Fikri, M.; Herzler, J.; Starke, R.; Schulz, C.; Roth, P.; Kalghatgi, G. Combust Flame 2008, 152, 276–281.
97. Dagaut, P.; Togbé, C. Energy Fuels 2009, 23, 3527–3535.
98. Saisirirat, P.; Togbé, C.; Chanchaona, S.; Foucher, F.; Mounaim-Rousselle, C.; Dagaut, P. Proc Combust Inst 2011, 33, 3007–3014.
99. Bissoli, M.; Frassoldati, A.; Cuoci, A.; Faravelli, T.; Ranzi, E. In Proceedings of the XXXVI Meeting of the Italian Section of the Combustion Institute, 2013.
100. Mze-Ahmed, A.; Hadj-Ali, K.; Dagaut, P.; Dayma, G. Energy Fuels 2012, 26, 4253–4268.
101. Davidson, D. F.; Hong, Z.; Pilla, G. L.; Farooq, A.; Cook, R. D.; Hanson, R. K. Proc Combust Inst 2011, 33, 151–157.
102. Darcy, D.; Nakamura, H.; Tobin, C.; Mehl, M.; Metcalfe, W.; Pitz, W.; Westbrook, C.; Curran, H. Combust Flame 2014, 161, 65–74.
103. Kim, H. H.; Diévart, P.; Santner, J.; Won, S. H.; Dooley, S.; Ju, Y. In 50th AIAA Aerospace Sciences Meeting Including the New Horizons Forum and Aerospace Exposition; American Institute of Aeronautics and Astronautics: Reston, VA, 2012.
104. Metcalfe, W. K.; Dooley, S.; Dryer, F. L. Energy Fuels 2011, 25, 4915–4936.
105. Hui, X.; Das, A. K.; Kumar, K.; Sung, C.-J.; Dooley, S.; Dryer, F. L. Fuel 2012, 97, 695–702.
106. Diévart, P.; Kim, H. H.; Won, S. H.; Ju, Y.; Dryer, F. L.; Dooley, S.; Wang, W.; Oehlschlaeger, M. A. Fuel 2013, 109, 125–136.
107. Seshadri, K.; Frassoldati, A.; Cuoci, A.; Faravelli, T.; Niemann, U.; Weydert, P.; Ranzi, E. Combust Theory Model 2011, 15, 569–583.
108. Comandini, A.; Dubois, T.; Abid, S.; Chaumeix, N. Energy Fuels 2013, 28, 714–724.
109. Li, B.; Zhang, H.; Egolfopoulos, F. N. Combust Flame 2014, 161, 154–161.
110. Ji, C.; Dames, E.; Sirjean, B.; Wang, H.; Egolfopoulos, F. N. Proc Combust Inst 2011, 33, 971–978.
111. Wu, F.; Kelley, A. P.; Law, C. K. Combust Flame 2012, 159, 1417–1425.
112. Zhu, Y.; Davidson, D. F.; Hanson, R. K. Combust Flame 2014, 161, 371–383.
113. Denman, B. M.; Munzar, J. D.; Bergthorson, J. M. InASME Turbo Expo 2012: Turbine Technical Conference and Exposition, 2012, pp. 1417–1426.
114. Kumar, K.; Sung, C.-J.; Hui, X. Fuel 2011, 90, 1004–1011.
115. Chong, C. T.; Hochgreb, S. Proc Combust Inst 2011, 33, 979–986.
116. Shen, H.-P. S.; Oehlschlaeger, M. A. Combust Flame 2009, 156, 1053–1062.
117. Won, S. H.; Dooley, S.; Veloo, P. S.; Wang, H.; Oehlschlaeger, M. A.; Dryer, F. L.; Ju, Y. Combust Flame 2014, 161(3), 826-834.
118. Pitsch, H. InSymposium (International) on Combustion, 1996, pp 721–728.
119. Pfahl, U.; Adomeit, G. SAE Paper 970897, 1997.
120. Barths, H.; Hasse, C.; Peters, N. Int J Engine Res 2000, 1, 249–267.
121. Bounaceur, R.; Glaude, P.-A.; Fournet, R.; Battin-Leclerc, F.; Jay, S.; Cruz, A., Int J Vehicle Des 2007, 44, 124–142.
122. Ramirez, H. P.; Hadj-Ali, K.; Dievart, P.; Moreac, G.; Dagaut, P. Energy Fuels 2010, 24, 1668–1676.

123. Wang, H.; Warner, S. J.; Oehlschlaeger, M. A.; Bounaceur, R.; Biet, J.; Glaude, P.-A.; Battin-Leclerc, F. Combust Flame 2010, 157, 1976–1988.
124. Pfahl, U.; Fieweger, K.; Adomeit, G. In Symposium (International) on Combustion, 1996, pp 781–789.
125. Shen, H.-P. S.; Steinberg, J.; Vanderover, J.; Oehlschlaeger, M. A. Energy Fuels 2009, 23, 2482–2489.
126. Herbinet, O.; Biet, J.; Hakka, M. H.; Warth, V.; Glaude, P.-A.; Nicolle, A.; Battin-Leclerc, F. Proc Combust Inst 2011, 33, 391–398.
127. Stagni, A.; Saggese, C.; Bissoli, M.; Cuoci, A.; Frassoldati, A.; Faravelli, T.; Ranzi, E. Chem Eng Trans 2014, 34.
128. Lin, L.; Cunshan, Z.; Vittayapadung, S.; Xiangqian, S.; Mingdong, D. Appl Energy 2011, 88, 1020–1031.
129. Campbell, M.; Davidson, D.; Hanson, R. In the 8th U. S. National Combustion Meeting, 2013, pp. 22–35.
130. Wang, W.; Oehlschlaeger, M. A. Combust Flame 2012, 159, 476–481.
131. Campbell, M.; Davidson, D. F.; Hanson, R. K.; Westbrook, C. K. Proc Combust Inst 2013, 34, 419–425.
132. Dagaut, P.; Sahasrabudhe, M. Proc Combust Inst 2007, 31, 2955–2961.
133. Hakka, M. H.; Glaude, P.-A.; Herbinet, O.; Battin-Leclerc, F. Combust Flame 2009, 156, 2129–2144.
134. Bax, S.; Hakka, M. H.; Glaude, P.-A.; Herbinet, O.; Battin-Leclerc, F. Combust Flame 2010, 157, 1220–1229.
135. Smith, G. P.; Golden, D. M.; Frenklach, M.; Moriarty, N. W.; Eiteneer, B.; Goldenberg, M.; Bowman, C. T.; Hanson, R. K.; Song, S.; Gardiner, W. C., Jr. GRI-Mech. Available at http://www.me.berkeley.edu/gri-mech/. Last visited March 2011.
136. Prince, J. C.; Williams, F. A. Combust Flame 2012, 159, 2336–2344.
137. Wang, H.; You, X.; Joshi, A. V.; Davis, S. G.; Laskin, A.; Egolfopoulos, F.; Law, C. K. USC Mech Version II, CO/C1-C4 Compounds, 2007.
138. Metcalfe, W. K.; Burke, S. M.; Ahmed, S. S.; Curran, H. J. Int J Chem Kinet 2013, 45, 638–675.
139. Smith, G. P.; Golden, D. M.; Frenklach, M.; Moriarty, N. W.; Eiteneer, B.; Goldenberg, M.; Bowman, C. T.; Hanson, R. K.; Song, S.; Gardiner W. C., Jr. Available at http://www.me.berkeley.edu/gri-mech, 1999, 51, 55.
140. Frenklach, M. Proc Combust Inst 2007, 31, 125–140.
141. Naik, C. V.; Puduppakkam, K. V.; Meeks, E. J Eng Gas Turbines Power 2012, 134, 021504.
142. Gustavsson, J.; Golovitchev, V. I. SAE Paper 1848, 2003.
143. Hernandez, J. J.; Sanz-Argent, J.; Benajes, J.; Molina, S. Fuel 2008, 87, 655–665.
144. Hentschel, W.; Schindler, K.-P.; Haahtela, O. Power 1994, 2002, 09–30.
145. Barths, H.; Hasse, C.; Bikas, G.; Peters, N. Proc Combust Inst 2000, 28, 1161–1168.
146. Lemaire, R.; Faccinetto, A.; Therssen, E.; Ziskind, M.; Focsa, C.; Desgroux, P. Proc Combust Inst 2009, 32, 737–744.
147. Seshadri, K. DTIC Document, 2003.
148. Li, B.; Liu, N.; Zhao, R.; Egolfopoulos, F. N.; Zhang, H. J Propul Power 2013, 29, 352–361.
149. Ra, Y.; Reitz, R. D. Combust Flame 2011, 158, 69–90.
150. Davis, S. G.; Law, C. K. Combust Sci Technol 1998, 140, 427–449.
151. Hirasawa, T.; Sung, C. J.; Joshi, A.; Yang, Z.; Wang, H.; Law, C. K. Proc Combust Inst 2002, 29, 1427–1434.
152. Kelley, A. P.; Smallbone, A. J.; Zhu, D. L.; Law, C. K. Proc Combust Inst 2011, 33, 963–970.
153. Huang, Y.; Sung, C. J.; Eng, J. A. Combust Flame 2004, 139, 239–251.
154. Johnston, R.; Farrell, J. Proc Combust Inst 2005, 30, 217–224.
155. Egolfopoulos, F.; Du, D.; Law, C. Combust Sci Technol 1992, 83, 33–75.
156. Veloo, P. S.; Wang, Y. L.; Egolfopoulos, F. N.; Westbrook, C. K. Combust Flame 2010, 157, 1989–2004.
157. Vancoillie, J.; Christensen, M.; Nilsson, E.; Verhelst, S.; Konnov, A. Energy Fuels 2012, 26, 1557–1564.
158. Dirrenberger, P.; Glaude, P.-A.; Bounaceur, R.; Le Gall, H.; da Cruz, A. P.; Konnov, A.; Battin-Leclerc, F. Fuel 2014, 115, 162–169.
159. Van Lipzig, J.; Nilsson, E.; De Goey, L.; Konnov, A. Fuel 2011, 90, 2773–2781.
160. Konnov, A.; Meuwissen, R.; De Goey, L. Proc Combust Inst 2011, 33, 1011–1019.
161. Zhukov, V. P.; Sechenov, V. A.; Starikovskii, A. Y. Combust Flame 2008, 153, 130–136.